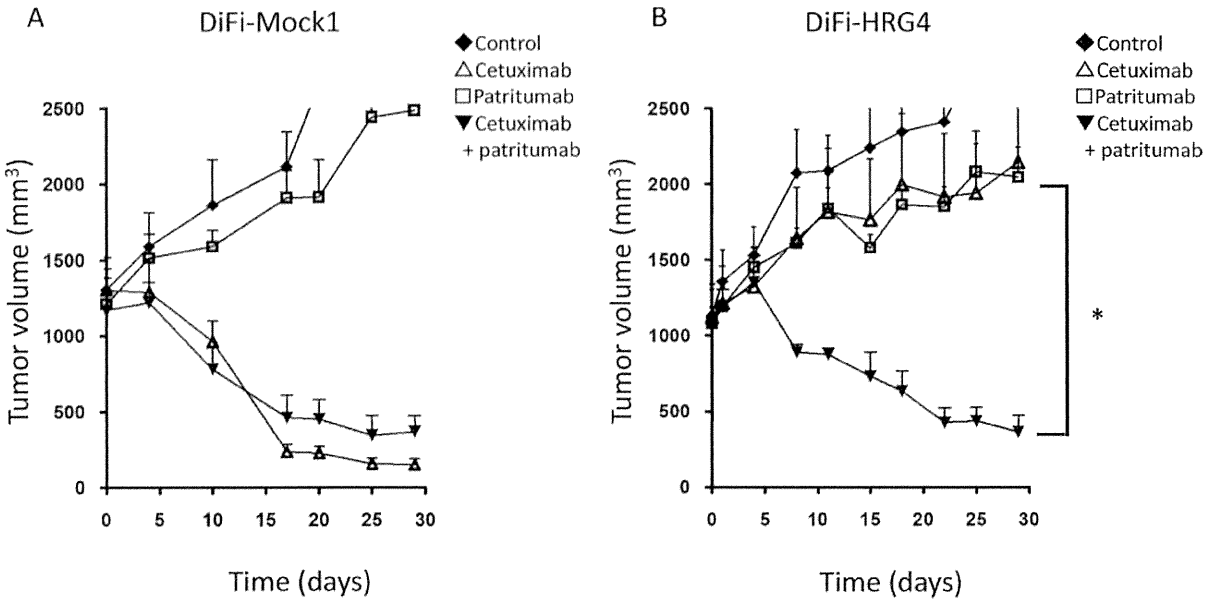

Figure 4: Effects of cetuximab, patritumab, and the combination of both drugs on the growth of DiFi-HRG tumor xenografts *in vivo*. Nude mice with tumor xenografts established by subcutaneous injection of DiFi-Mock1 (**A**) or DiFi-HRG4 (**B**) cells were treated for 4 weeks with vehicle (control), cetuximab (1.0 mg/body), patritumab (1.0 mg/body), or both drugs, as described in Materials and Methods. Tumor volume was determined at the indicated times after the onset of treatment. Data are means ± SE from six mice per group. $^*P < 0.05$ for comparison of the combination of both drugs with cetuximab alone or patritumab alone (Student's *t* test).

therapy [8]. Effective treatment options to overcome cetuximab resistance mediated by heregulin are thus urgently required.

We have here established heregulin-overexpressing sublines of DiFi cells (DiFi-HRG cells) and shown that these cells are resistant to cetuximab both *in vitro* and *in vivo*. Whereas the amount of the transmembrane form of heregulin was substantially higher in DiFi-HRG4 cells than in DiFi-HRG5 or DiFi-HRG6 cells (Fig. 1A), these three cell lines appeared to release similar amounts of the soluble form of heregulin into the culture medium (Fig. 1B). This difference in the relative abundance of the transmembrane and soluble forms of heregulin among DiFi-HRG cell lines might reflect a difference in the activity of cell surface proteases among the cell lines. Alternatively, the production of the transmembrane form of heregulin in DiFi-HRG4 cells might exceed the capacity of such proteases. To investigate the mechanism responsible for cetuximab resistance in DiFi-HRG cells, we examined differences in signal transduction between these cells and DiFi-Mock1 cells. In DiFi-Mock1 cells, cetuximab inhibited the phosphorylation of EGFR, HER2, HER3, AKT, and ERK as well as up-regulated BIM expression and down-regulated survivin expression, resulting in the induction of apoptosis. By contrast, in DiFi-HRG cell lines, whereas cetuximab inhibited EGFR and ERK phosphorylation, leading to BIM induction, it did not affect HER2, HER3, or AKT phosphorylation or survivin expression. Given that down-regulation both of AKT signaling and of the expression of its downstream target survivin is required for apoptosis induced by inhibition of receptor tyrosine kinases [14–16], our data suggest that sustained AKT-survivin signaling in the presence of cetuximab is responsible for the resistance of DiFi-HRG cell lines to this drug. To investigate further the relation between AKT signaling and the operation of a heregulin autocrine loop, we examined the effects of patritumab, a neutralizing monoclonal antibody to HER3, in DiFi-HRG4 cells. We found that exposure of these cells to patritumab in combination with cetuximab resulted in inhibition of EGFR, HER2, HER3, AKT, and ERK phosphorylation as well as in both up-regulation of BIM expression and down-regulation of survivin expression, leading to the induction of apoptosis. These results indicate that AKT signaling is triggered by heregulin binding to HER3.

Given that HER3 (a kinase-dead receptor) manifests impaired kinase activity [21], it requires dimerization with other HER family members to activate signaling after ligand binding [22, 23]. HER2 has been implicated as a dimerization partner of HER3, and heregulin stabilizes the HER2-HER3 heterodimer [9]. In this context, we examined the effects of lapatinib, a TKI for EGFR and HER2, in DiFi-HRG4 cells. Inhibition of EGFR and HER2 by lapatinib resulted in down-regulation of HER3, AKT, and ERK phosphorylation as well as in the induction of BIM and suppression of survivin expression in these cells, thereby triggering apoptosis (Supplementary Fig. S1A, S1B). These

findings suggest that, in DiFi-HRG cells, HER3 is trans-phosphorylated by HER2 as a result of heregulin-induced HER2-HER3 heterodimerization, which in turn leads to the activation of AKT signaling [24] (Fig. 5A, 5B, 5C). The heterodimerization partner of HER3 is thus likely switched from EGFR to HER2 as a result of the overexpression of heregulin in DiFi-HRG cells. We also found that patritumab alone inhibited the phosphorylation of HER3 and AKT as well as down-regulated survivin expression in DiFi-HRG4 cells but not in DiFi-Mock1 cells (Fig. 3D, 3E). These results suggest that patritumab may prevent ligand-dependent HER3 phosphorylation by blocking HER2-HER3 heterodimerization, whereas it has little effect on ligand-independent HER3 phosphorylation.

In our DiFi-HRG xenograft model, we showed that combination therapy with patritumab and cetuximab inhibited tumor growth to the same extent as did cetuximab alone in the DiFi-Mock1 xenograft model. Antagonism of the heregulin-HER3 interaction by patritumab thus represents an effective strategy to abrogate cetuximab resistance induced by heregulin derived from tumor cells. Given that elevated circulating levels of heregulin are associated with both de novo and acquired cetuximab resistance in mCRC patients [8], our model systems based on stable overexpression of heregulin are clinically relevant and should prove useful for establishing strategies to overcome cetuximab resistance mediated by the heregulin autocrine loop. Indeed, a recent phase I/II study with refractory colorectal cancer patients revealed potential antitumor activity of the combination of cetuximab and pertuzumab, a HER2-targeted antibody that blocks ligand-dependent HER2-HER3 heterodimerization. However, this drug combination was not tolerable as a result of overlapping toxicities [25]. Given that the toxicity profile of patritumab differs from that of pertuzumab [26], the combination of cetuximab and patritumab warrants evaluation in the clinical setting. We also found that the IC_{50} value for the antiproliferative effect of the combination of cetuximab and patritumab in DiFi-HRG4 cells was ~10 times as high as that for cetuximab alone in DiFi-Mock1 cells (Fig. 1C, Fig. 3A). The discrepancy between these *in vitro* data and our *in vivo* findings may suggest that antibody-dependent cellular cytotoxicity [27] involving NK cell activation plays a role in tumor growth inhibition by the combination of both agents. Moreover, combination therapy with these two IgG1 antibodies may result in an enhanced antitumor activity mediated by cytotoxic T lymphocytes [28] in the clinical setting. Given the recent evidence implicating the importance of interactions between therapeutic antibodies and the immune system in the efficacy of antibody treatment [20], further investigation of such mechanisms is warranted.

In conclusion, we have shown that consecutive activation of HER2-HER3 and AKT by heregulin in an autocrine-dependent manner confers resistance to cetuximab, and that patritumab restores cetuximab sensitivity in tumors with heregulin-induced cetuximab resistance. Further studies of combination therapy with patritumab and cetuximab are thus warranted in mCRC patients with heregulin-induced resistance to EGFR-targeted antibodies.

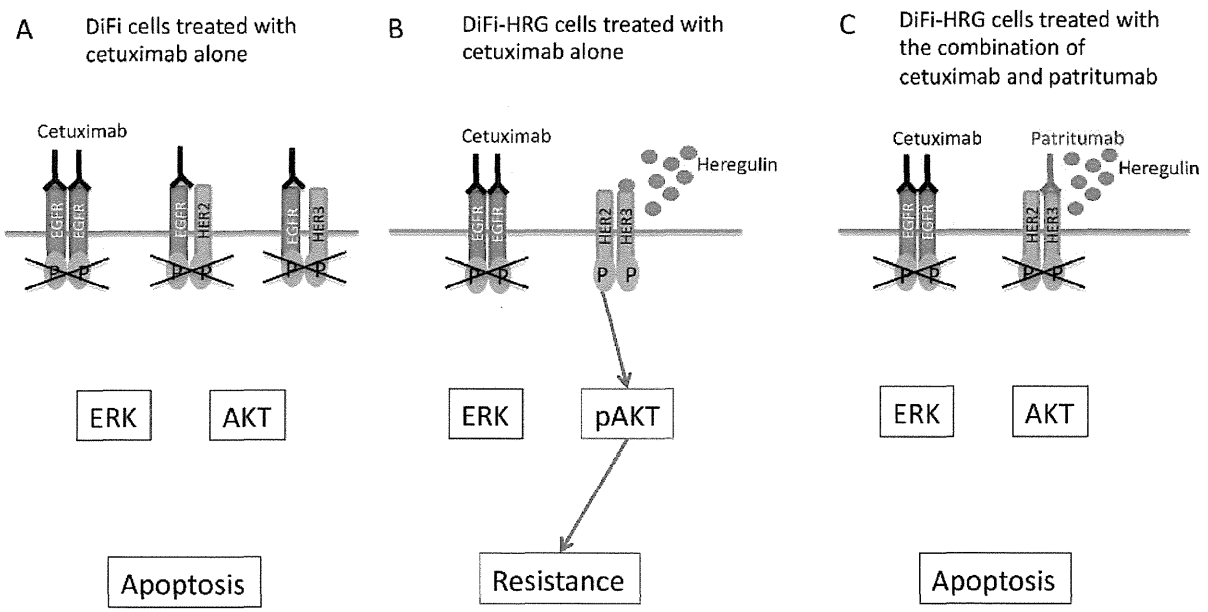

Figure 5: Model for intracellular signaling underlying the induction of apoptosis by cetuximab and patritumab in colorectal cancer cells. **(A)** DiFi colorectal cancer cells treated with cetuximab alone. **(B)** DiFi cells that stably overexpress heregulin (DiFi-HRG cells) are resistant to cetuximab as a result of HER2-HER3 heterodimerization and AKT activation induced by heregulin. **(C)** Patritumab abrogates cetuximab resistance mediated by the heregulin autocrine loop in DiFi-HRG cells.

MATERIALS AND METHODS

Cells and reagents

The DiFi human colorectal cancer cell line was kindly provided by P. A. Janne (Dana Farber Cancer Institute). DiFi cells were maintained under a humidified atmosphere of 5% CO_2 in air at 37°C in Dulbecco's modified Eagle's medium (DMEM) containing high glucose and supplemented with Ham's F-12 and 10% fetal bovine serum (FBS). Cetuximab was obtained from Merck Serono, and patritumab was kindly provided by Daiichi-Sankyo (Tokyo, Japan). Recombinant human heregulin (NRG1-β1/HRG1-β1 extracellular domain) was obtained from R&D Systems.

Establishment of cells stably overexpressing heregulin

A full-length cDNA encoding human heregulin (NRG1, GenBank accession no. NM_013956) was obtained from Origene (Rockville, MD). The amplification product was verified by sequencing after its cloning into the pCR-Blunt II-TOPO vector (Invitrogen). The heregulin cDNA was then excised from pCR-Blunt II-TOPO and transferred to the pQCXIH retroviral vector (Clontech), and retroviruses encoding heregulin were produced and used to infect DiFi cells as described [29]. Cells stably expressing heregulin were then isolated by selection with hygromycin (Invivogen) at 500 μg/mL.

Cell growth inhibition assay

Cells were transferred to 96-well flat-bottomed plates and cultured for 24 h before exposure to various concentrations of cetuximab or patritumab in medium containing 1% FBS for 120 h. Cell Counting Kit-8 solution (Dojindo, Kumamoto, Japan) was then added to each well, and the cells were incubated for 3 h at 37°C before measurement of absorbance at 490 nm with a Multiskan Spectrum instrument (Thermo Labsystems). Absorbance values were expressed as a percentage of that for nontreated cells, and the IC_{50} of cetuximab for inhibition of cell growth was determined.

Heregulin ELISA

The concentration of heregulin in cell culture supernatants was measured with the use of a sandwich ELISA (NRG1-β1 DuoSet, R&D Systems) as previously described [30]. Cells were seeded in six-well plates at a density of 0.5×10^6 cells per well in DMEM supplemented with 10% FBS. After the cells had achieved confluence, the medium was replaced with 5 ml of DMEM supplemented with 0.1% FBS, the cells were incubated for 48 h, and the culture supernatants were collected for assay of heregulin.

Immunoblot analysis

Cells were washed twice with ice-cold phosphate-buffered saline (PBS) and then lysed with 1 × Cell Lysis Buffer (Cell Signaling Technology) consisting of 20 mmol/L Tris-HCl (pH 7.5), 150 mmol/L NaCl, 1 mmol/L EDTA (disodium salt), 1 mmol/L EGTA, 1% Triton X-100, 2.5 mmol/L sodium pyrophosphate, 1 mmol/L β-glycerophosphate, 1 mmol/L Na_3VO_4, leupeptin (1 μg/mL), and 1 mmol/L phenylmethylsulfonyl fluoride. The protein concentration of the lysates was determined with a bicinchoninic acid assay kit (Thermo Fisher Scientific), and equal amounts of protein were subjected to SDS-polyacrylamide gel electrophoresis on a 7.5% gel (Bio-Rad). The separated proteins were transferred to a nitrocellulose membrane, which was then incubated with Blocking One solution (Nacalai Tesque) for 20 min at room temperature before incubation overnight at 4°C with primary antibodies. Antibodies to heregulin (NRG1-β1), to phosphorylated EGFR (phospho-Tyr[1068]), to phosphorylated HER2 (phospho-Tyr[1248]), to phosphorylated HER3 (phospho-Tyr[1289]), to phosphorylated or total forms of AKT, to phosphorylated ERK, to PARP, and to BIM were obtained from Cell Signaling Technology; those to total HER3, to total ERK, and to survivin were from Santa Cruz Biotechnology; those to total EGFR were from Zymed/Invitrogen; those to total HER2 were from Millipore; and those to β-actin were from Sigma. The membrane was then washed with PBS containing 0.05% Tween 20 before incubation for 1 h at room temperature with horseradish peroxidase–conjugated secondary antibodies (GE Healthcare). Immune complexes were finally detected with ECL detection reagents (GE Healthcare).

Annexin V binding assay

The binding of annexin V to cells was measured with the use of an Annexin-V-FLUOS Staining Kit (Roche). Cells were harvested by exposure to trypsin-EDTA, washed with PBS, and centrifuged at 200 × *g* for 5 min. The cell pellets were resuspended in 100 μL of Annexin-V-FLUOS labeling solution, incubated for 10 to 15 min at 15° to 25°C, and then analyzed for fluorescence with a flow cytometer (FACSCalibur) and Cell Quest software (Becton Dickinson).

Tumor growth inhibition assay *in vivo*

All animal experiments were performed in accordance with the Recommendations for Handling of Laboratory Animals for Biomedical Research compiled by the Committee on Safety and Ethical Handling Regulations for Laboratory Animal Experiments, Kinki University. The ethical procedures followed conformed to the UKCCCR guidelines for the welfare and use of

animals in cancer research [31]. The study was also reviewed and approved by the Animal Ethics Committee of Kinki University (approval no. KAME-22-018). Cells were injected subcutaneously into the axilla of 5- to 6-week-old female athymic nude mice (BALB/c nu/nu; CLEA Japan), and treatment was initiated when tumors in each group of six mice achieved an average volume of 1000 to 1200 mm^3. Treatment groups consisted of vehicle control, cetuximab (1.0 mg/body), patritumab (1.0 mg/body), and the combination of both agents. Cetuximab and patritumab were administered by intraperitoneal injection twice a week for 4 weeks, with control animals receiving a 0.5% (w/v) aqueous solution of hydroxyl propylmethyl cellulose as vehicle. Tumor volume was determined from caliper measurements of tumor length (L) and width (W) according to the formula $LW^2/2$. Both tumor size and body weight were measured twice weekly. For ethical reasons, animals were removed from the study if the tumor volume exceeded 2500 mm^3.

Statistical analysis

Quantitative data are presented as means ± SE unless indicated otherwise. The significance of differences was evaluated with the unpaired two-tailed Student's t test. A P value of < 0.05 was considered statistically significant.

Conflict of interest statement

The authors declare no conflict of interest.

REFERENCES

1. Van Cutsem E, Kohne CH, Hitre E, Zaluski J, Chang Chien CR, Makhson A, D'Haens G, Pinter T, Lim R, Bodoky G, Roh JK, Folprecht G, Ruff P, Stroh C, Tejpar S, Schlichting M, et al. Cetuximab and chemotherapy as initial treatment for metastatic colorectal cancer. N Engl J Med. 2009; 360:1408–1417.
2. Bokemeyer C, Bondarenko I, Makhson A, Hartmann JT, Aparicio J, de Braud F, Donea S, Ludwig H, Schuch G, Stroh C, Loos AH, Zubel A, Koralewski P. Fluorouracil, leucovorin, and oxaliplatin with and without cetuximab in the first-line treatment of metastatic colorectal cancer. J Clin Oncol. 2009; 27:663–671.
3. Tol J, Koopman M, Cats A, Rodenburg CJ, Creemers GJ, Schrama JG, Erdkamp FL, Vos AH, van Groeningen CJ, Sinnige HA, Richel DJ, Voest EE, Dijkstra JR, Vink-Borger ME, Antonini NF, Mol L, et al. Chemotherapy, bevacizumab, and cetuximab in metastatic colorectal cancer. N Engl J Med. 2009; 360:563–572.
4. Di Nicolantonio F, Martini M, Molinari F, Sartore-Bianchi A, Arena S, Saletti P, De Dosso S, Mazzucchelli L, Frattini M, Siena S, Bardelli A. Wild-type BRAF is required for response to panitumumab or cetuximab in metastatic colorectal cancer. J Clin Oncol. 2008; 26:5705–5712.
5. Montagut C, Dalmases A, Bellosillo B, Crespo M, Pairet S, Iglesias M, Salido M, Gallen M, Marsters S, Tsai SP, Minoche A, Seshagiri S, Serrano S, Himmelbauer H, Bellmunt J, Rovira A, et al. Identification of a mutation in the extracellular domain of the Epidermal Growth Factor Receptor conferring cetuximab resistance in colorectal cancer. Nat Med. 2012; 18:221–223.
6. Misale S, Yaeger R, Hobor S, Scala E, Janakiraman M, Liska D, Valtorta E, Schiavo R, Buscarino M, Siravegna G, Bencardino K, Cercek A, Chen CT, Veronese S, Zanon C, Sartore-Bianchi A, et al. Emergence of KRAS mutations and acquired resistance to anti-EGFR therapy in colorectal cancer. Nature. 2012; 486:532–536.
7. Bardelli A, Corso S, Bertotti A, Hobor S, Valtorta E, Siravegna G, Sartore-Bianchi A, Scala E, Cassingena A, Zecchin D, Apicella M, Migliardi G, Galimi F, Lauricella C, Zanon C, Perera T, et al. Amplification of the MET receptor drives resistance to anti-EGFR therapies in colorectal cancer. Cancer Discov. 2013; 3:658–673.
8. Yonesaka K, Zejnullahu K, Okamoto I, Satoh T, Cappuzzo F, Souglakos J, Ercan D, Rogers A, Roncalli M, Takeda M, Fujisaka Y, Philips J, Shimizu T, Maenishi O, Cho Y, Sun J, et al. Activation of ERBB2 signaling causes resistance to the EGFR-directed therapeutic antibody cetuximab. Sci Transl Med. 2011; 3:99ra86.
9. Wallasch C, Weiss FU, Niederfellner G, Jallal B, Issing W, Ullrich A. Heregulin-dependent regulation of HER2/neu oncogenic signaling by heterodimerization with HER3. EMBO J. 1995; 14:4267–4275.
10. Gala K, Chandarlapaty S. Molecular pathways: HER3 targeted therapy. Clin Cancer Res. 2014; 20:1410–1416.
11. Freeman D, Ogbagabreiel S, Rothe M, Radinsky R, Treder M. 2008; Fully human Anti-HER3 monoclonal antibodies (mAbs) have unique *in vitro* and *in vivo* functional and antitumor activities versus other HER family inhibitors (abstract). Proceedings of the Annual Meeting of the American Association for Cancer Research; San Diego, CA: AACR.
12. Treder M, Hartmann S, Ogbagabrei S, Borges E, Green L, Kang Jea (2008); Fully human Anti-HER3 monoclonal antibodies (mAbs) inhibit oncogenic signaling and tumor cell growth *in vitro* and vivo. Proceedings of the Annual Meeting of the American Association for Cancer Research; San Diego, CA.: AACR.
13. McDermott U, Sharma SV, Dowell L, Greninger P, Montagut C, Lamb J, Archibald H, Raudales R, Tam A, Lee D, Rothenberg SM, Supko JG, Sordella R, Ulkus LE, Iafrate AJ, Maheswaran S, et al. Identification of genotype-correlated sensitivity to selective kinase inhibitors by using high-throughput tumor cell line profiling. Proc Natl Acad Sci U S A. 2007; 104:19936–19941.
14. Okamoto K, Okamoto I, Okamoto W, Tanaka K, Takezawa K, Kuwata K, Yamaguchi H, Nishio K,

Nakagawa K. Role of survivin in EGFR inhibitor-induced apoptosis in non-small cell lung cancers positive for EGFR mutations. Cancer Res. 2010; 70:10402–10410.

15. Tanizaki J, Okamoto I, Fumita S, Okamoto W, Nishio K, Nakagawa K. Roles of BIM induction and survivin downregulation in lapatinib-induced apoptosis in breast cancer cells with HER2 amplification. Oncogene. 2011; 30:4097–4106.
16. Okamoto W, Okamoto I, Arao T, Kuwata K, Hatashita E, Yamaguchi H, Sakai K, Yanagihara K, Nishio K, Nakagawa K. Antitumor action of the MET tyrosine kinase inhibitor crizotinib (PF-02341066) in gastric cancer positive for MET amplification. Mol Cancer Ther. 2012; 11:1557–1564.
17. Siena S, Sartore-Bianchi A, Di Nicolantonio F, Balfour J, Bardelli A. Biomarkers predicting clinical outcome of epidermal growth factor receptor-targeted therapy in metastatic colorectal cancer. J Natl Cancer Inst. 2009; 101:1308–1324.
18. De Roock W, De Vriendt V, Normanno N, Ciardiello F, Tejpar S. KRAS, BRAF, PIK3CA, and PTEN mutations: implications for targeted therapies in metastatic colorectal cancer. Lancet Oncol. 2011; 12:594–603.
19. Bardelli A, Siena S. Molecular mechanisms of resistance to cetuximab and panitumumab in colorectal cancer. J Clin Oncol. 2010; 28:1254–1261.
20. Troiani T, Zappavigna S, Martinelli E, Addeo SR, Stiuso P, Ciardiello F, Caraglia M. Optimizing treatment of metastatic colorectal cancer patients with anti-EGFR antibodies: overcoming the mechanisms of cancer cell resistance. Expert Opin Biol Ther. 2013; 13:241–255.
21. Guy PM, Platko JV, Cantley LC, Cerione RA, Carraway KL, 3rd . Insect cell-expressed p180erbB3 possesses an impaired tyrosine kinase activity. Proc Natl Acad Sci U S A. 1994; 91:8132–8136.
22. Holbro T, Beerli RR, Maurer F, Koziczak M, Barbas CF, 3rd, Hynes NE. The ErbB2/ErbB3 heterodimer functions as an oncogenic unit: ErbB2 requires ErbB3 to drive breast tumor cell proliferation. Proc Natl Acad Sci U S A. 2003; 100:8933–8938.
23. Knowlden JM, Hutcheson IR, Jones HE, Madden T, Gee JM, Harper ME, Barrow D, Wakeling AE, Nicholson RI. Elevated levels of epidermal growth factor receptor/c-erbB2 heterodimers mediate an autocrine growth regulatory pathway in tamoxifen-resistant MCF-7 cells. Endocrinology. 2003; 144:1032–1044.
24. Tzahar E, Waterman H, Chen X, Levkowitz G, Karunagaran D, Lavi S, Ratzkin BJ, Yarden Y. A hierarchical network of interreceptor interactions determines signal transduction by Neu differentiation factor/neuregulin and epidermal growth factor. Mol Cell Biol. 1996; 16:5276–5287.
25. Rubinson DA, Hochster HS, Ryan DP, Wolpin BM, McCleary NJ, Abrams TA, Chan JA, Iqbal S, Lenz HJ, Lim D, Rose J, Bekaii-Saab T, Chen HX, Fuchs CS, Ng K. Multi-drug inhibition of the HER pathway in metastatic colorectal cancer: results of a phase I study of pertuzumab plus cetuximab in cetuximab-refractory patients. Invest New Drugs. 2014; 32:113–122.
26. LoRusso P, Janne PA, Oliveira M, Rizvi N, Malburg L, Keedy V, Yee L, Copigneaux C, Hettmann T, Wu CY, Ang A, Halim AB, Beckman RA, Beaupre D, Berlin J. Phase I Study of U3-1287, a Fully Human Anti-HER3 Monoclonal Antibody, in Patients with Advanced Solid Tumors. Clin Cancer Res. 2013; 19:3078–3087.
27. Kimura H, Sakai K, Arao T, Shimoyama T, Tamura T, Nishio K. Antibody-dependent cellular cytotoxicity of cetuximab against tumor cells with wild-type or mutant epidermal growth factor receptor. Cancer Sci. 2007; 98:1275–1280.
28. Correale P, Botta C, Cusi MG, Del Vecchio MT, De Santi MM, Gori Savellini G, Bestoso E, Apollinari S, Mannucci S, Marra M, Abbruzzese A, Aquino A, Turriziani M, Bonmassar L, Caraglia M, Tagliaferri P. Cetuximab +/– chemotherapy enhances dendritic cell-mediated phagocytosis of colon cancer cells and ignites a highly efficient colon cancer antigen-specific cytotoxic T-cell response *in vitro*. Int J Cancer. 2012; 130:1577–1589.
29. Tanaka K, Arao T, Maegawa M, Matsumoto K, Kaneda H, Kudo K, Fujita Y, Yokote H, Yanagihara K, Yamada Y, Okamoto I, Nakagawa K, Nishio K. SRPX2 is overexpressed in gastric cancer and promotes cellular migration and adhesion. Int J Cancer. 2009; 124:1072–1080.
30. Yonesaka K, Zejnullahu K, Lindeman N, Homes AJ, Jackman DM, Zhao F, Rogers AM, Johnson BE, Janne PA. Autocrine production of amphiregulin predicts sensitivity to both gefitinib and cetuximab in EGFR wild-type cancers. Clin Cancer Res. 2008; 14:6963–6973.
31. Workman P, Aboagye EO, Balkwill F, Balmain A, Bruder G, Chaplin DJ, Double JA, Everitt J, Farningham DA, Glennie MJ, Kelland LR, Robinson V, Stratford IJ, Tozer GM, Watson S, Wedge SR, et al. Guidelines for the welfare and use of animals in cancer research. Br J Cancer. 2010; 102:1555–1577.

Chemistry & Biology
Article

Balance between Exocytosis and Endocytosis Determines the Efficacy of Sterol-Targeting Antibiotics

Shinichi Nishimura,[1,*] Masato Tokukura,[1] Junko Ochi,[1] Minoru Yoshida,[2] and Hideaki Kakeya[1,*]
[1]Division of Bioinformatics and Chemical Genomics, Department of System Chemotherapy and Molecular Sciences, Graduate School of Pharmaceutical Sciences, Kyoto University, Kyoto 606-8501, Japan
[2]Chemical Genomics Research Group, RIKEN Center for Sustainable Resource Science, Wako, Saitama 351-0198, Japan
*Correspondence: nshin@pharm.kyoto-u.ac.jp (S.N.), scseigyo-hisyo@pharm.kyoto-u.ac.jp (H.K.)
http://dx.doi.org/10.1016/j.chembiol.2014.10.014

SUMMARY

Antifungals targeting membrane ergosterol are longstanding, yet indispensable drugs in clinical use. However, the mechanisms by which the cellular membrane domains recognized by these antibiotics are generated remain largely unknown. Here, we demonstrate that the balance between endocytosis and exocytosis in membrane trafficking is a critical factor in the action of sterol-targeting antibiotics. When fission yeast cells were treated with manumycin A, cellular binding and the action of the antifungals filipin, amphotericin B, and theonellamides, all of which are ergosterol-binders, were abolished. Additionally, manumycin A treatment attenuated Cdc42 activity and inhibited exocytosis, while endocytosis was only moderately suppressed. Similar defects in membrane trafficking could be reproduced by heat shock and genetic perturbation, which also abolished the action of the antibiotics. We propose that exocytosis and endocytosis respectively supply and internalize the specific plasma membrane domains recognized by sterol-targeting antibiotics.

INTRODUCTION

The cell membrane serves as a physical barrier that defines the cell boundary and segregates the interior into distinct compartments, each performing a specialized function. Among the many lipid constituents of cell membranes, sterols are unique in that they are major regulators of membrane fluidity and thickness and contribute to the formation of specific membrane microdomains (Simons and Ikonen, 1997). Additionally, sterols are medically important molecules often targeted by antibiotics and toxins. Using artificial membranes, many studies have been carried out to gain insights into the action of sterol-targeting exogenous molecules. However, as yet, little is known about how antibiotics recognize the cellular membrane, and how the corresponding membrane domains are generated in the cell (Bolard, 1986; Gray et al., 2012). Cellular membranes are highly complex; it is therefore imperative to use the right model organism with clear-cut phenotypes to elucidate the basic mechanisms behind the construction of the living cell membrane.

The fission yeast *Schizosaccharomyces pombe* is a rod-shaped unicellular organism that grows by length extension at the cell tips, where actin patches, glucan synthases, and the processes of exocytosis and endocytosis are all concentrated (Hayles and Nurse, 2001). Sterol-rich domains in the plasma membrane have also been detected at the growing cell tips (Wachtler et al., 2003). Most of the components located at the cell tips during interphase, including these sterol-rich plasma membrane domains, are recruited to the site of cytokinesis for equal distribution upon cell division. Since the polarity of sterol-rich membrane domains in *S. pombe* cells can be clearly visualized using sterol probes and fluorescence microscopy (Nishimura et al., 2010; Wachtler et al., 2003), *S. pombe* is an excellent model organism for investigating the physical and biological nature of sterol-rich membrane domains. The polarized distribution of these domains is regulated in a cell cycle-dependent manner (Wachtler et al., 2003) and has been shown to require normal actin cytoskeleton organization (Codlin et al., 2008; Takeda et al., 2004), myosin type I (Myo1) protein (Takeda and Chang, 2005), and Cdc15, a contractile ring protein (Takeda et al., 2004).

In addition to the cytoskeletal machinery, the functional secretory pathway was also shown to be necessary for sterol-rich membrane domain distribution; in cell-cycle mutant *cdc25-22* cells, brefeldin A (BFA), an inhibitor of ER-to-Golgi transport (Graham et al., 1993), inhibited the appearance of sterol-rich domains (Wachtler et al., 2003). However, in wild-type cells, BFA treatment yielded rather bright fluorescent signals that lost polarity, raising the question of whether the functional secretory pathway alone is sufficient for generating polarized sterol localization (Figure S1A available online).

During the course of screening for chemical modulators of the action of membrane-targeting antibiotics, we found that manumycin A (manu-A) inhibited the binding of sterol-targeting antibiotics to fission yeast cells. Here, using manu-A as a chemical genetics tool, we demonstrate that the balance between exocytosis and endocytosis is critical for generating the membrane domains recognized by sterol-targeting antibiotics.

RESULTS AND DISCUSSION

Manu-A Abolishes the Cellular Binding of Sterol-Targeting Antibiotics

Sterol-rich domains in the plasma membrane can be visualized with filipin, a polyene antibiotic that exhibits fluorescence upon binding to membrane sterols (Drabikowski et al., 1973). To investigate how cellular membranes are recognized by sterol-targeting antibiotics, we tested a set of chemicals for their effect on filipin staining. We found that when cells were pretreated with manu-A (see structure in Figure 1A), the fluorescent signal from filipin was absent (Figure 1B). There are two possible mechanisms for this phenomenon: manu-A might quench the fluorescence of the filipin-sterol complexes, or it might sequester sterols, thereby hampering the formation of the filipin-sterol complexes. To investigate these possibilities, we tested the effect of manu-A on other sterol-targeting antibiotics. First, we tested amphotericin B (AmB), another polyene antibiotic that is commonly prescribed as an ergosterol-targeting antifungal drug (Volmer et al., 2010). AmB is known to induce large vacuoles in yeast cells, probably as a consequence of binding to ergosterol (Bhuiyan et al., 1999). However, this morphological change was suppressed when the cells were pretreated with manu-A (Figure 1C). Notably, the toxicity of filipin and AmB were also attenuated (Figure 1D). In fission yeast cells, filipin showed toxicity at 2 μg/ml and partially inhibited growth of the cells at 1 μg/ml. In the presence of manu-A, growth inhibition by filipin (1 μg/ml) was not observed, although it must be noted that cell growth was attenuated by manu-A across all filipin concentrations. The mitigating effect of manu-A on AmB toxicity was more distinct, as the minimum inhibitory concentration (MIC value) of AmB doubled in the presence of manu-A.

Next, we examined theonellamides (TNMs), bicyclic peptides isolated from marine sponges (Matsunaga and Fusetani, 1995; Matsunaga et al., 1989) that target membrane sterols (Espiritu et al., 2013). TNM fluorescent derivatives, such as TNM-aminomethylcoumarin acetate (AMCA), specifically recognize 3β-hydroxysterols. These fluorescent derivatives can therefore act as markers of 3β-hydroxysterols in both yeast (Ho et al., 2009; Nishimura et al., 2010) and cultured mammalian cells (Nishimura et al., 2013). TNM-AMCA treatment of the fission yeast cells exhibited polarized staining similar to that obtained with filipin, and this staining was also inhibited by pretreatment with manu-A (Figure 1E). Treatment of fission yeast cells with TNMs induces abnormal cell wall morphology (Nishimura et al., 2010). Consistent with the inhibition of the cellular binding of TNM-AMCA by manu-A, this abnormal cell wall phenotype was not observed following pretreatment with manu-A (data not shown). Additionally, growth inhibition by TNM-A was also attenuated (Figure 1D), and manu-A quadrupled the MIC value of this compound. Because filipin, AmB, and TNMs belong to different chemical classes based on their structure (Figure S2), the effect of manu-A is unlikely to be dependent on the chemical properties of the antibiotics. It is unlikely that the fluorescence of the filipin-sterol complexes was directly quenched by manu-A. Instead, it is likely that manu-A treatment sequesters antibiotic-targeted ergosterol molecules in the plasma membrane using as yet unknown mechanisms.

Manu-A was originally isolated from *Streptomyces parvulus* (Zeeck et al., 1987). This metabolite has been reported to inhibit several enzymes including caspase I (Tanaka et al., 1996) and neutral sphingomyelinase (Arenz et al., 2001), and protein farnesyltransferase (FTase) (Hara et al., 1993). It has also been observed to inhibit protein FTase in the budding yeast, *Saccharomyces cerevisiae* (Hara et al., 1993). We therefore examined the possibility that FTase inhibition is responsible for the effects of manu-A observed in *S. pombe*. Protein FTase consists of α and β subunits encoded by the *cwp1* and *cpp1* genes, respectively. FTase activity was abolished in cells lacking the *cpp1* gene (Yang et al., 2000), however, sterol-rich membrane domains were still observed to localize in a polarized manner, although polarity in the cell shape was severely reduced (Figure 1F) (Ma et al., 2006). Additionally, the sterol-rich domains of these mutant cells disappeared after treatment with manu-A. We also examined the *css1* gene, which encodes inositol phosphosphingolipid phospholipase C, a yeast counterpart of mammalian sphingomyelinase. Manu-A has been reported to inhibit neutral sphingomyelinase (Arenz et al., 2001). Sphingomyelinase catalyzes the hydrolysis of sphingomyelin to produce ceramide, which is required for membrane budding in liposomes and exocytosis in mammalian cells (Trajkovic et al., 2008). However, *css1* mutant cells did not reproduce the phenotype of manu-A treatment (Figure S3A). These results indicated that protein FTase and inositol phosphosphingolipid phospholipase C do not mediate the effect of manu-A on the plasma membrane.

Sterol Levels and Sterol-Rich Membrane Domains

The disappearance of sterol-rich domains from the plasma membrane can be caused by a decrease in sterol levels. We therefore measured the amount of ergosterol present in cells subsequent to treatment with manu-A, under the following two conditions. When cells were cultivated in a rich medium containing manu-A (1 μg/ml), the ergosterol level decreased to 77.7 ± 6.0% and no filipin signal was detected (Figure 1B). In contrast, when cells were cultivated in a synthetic medium, a lower concentration of manu-A (0.1 μg/ml) decreased the ergosterol level to a similar level of 75.6 ± 2.7%, although the filipin signal was still observed (Figure S3B). These results revealed that the amount of ergosterol present could not be correlated to the presence or absence of sterol-rich domains in the plasma membrane. We next compared the kinetics of the effect of manu-A and terbinafine, a potent inhibitor of squalene epoxidase, a requisite enzyme for ergosterol biosynthesis (Figures S3C and S3D). Compared with manu-A, a longer incubation period (more than 5 h) with terbinafine was required before the sterol-rich membrane domains were observed to disappear. These results suggested that a decrease in ergosterol was not responsible for the disappearance of sterol-rich membrane domains in the presence of manu-A. The decreased ergosterol levels affected by manu-A may be a result of feedback regulation following dysregulation of membrane trafficking (as discussed further below). As a case in point, cells lacking the *apm1* gene, which encodes the AP-1 adaptor complex μ subunit involved in vesicle-mediated transport, are known to contain only about 50% of ergosterol due to an unknown mechanism (Fang et al., 2012).

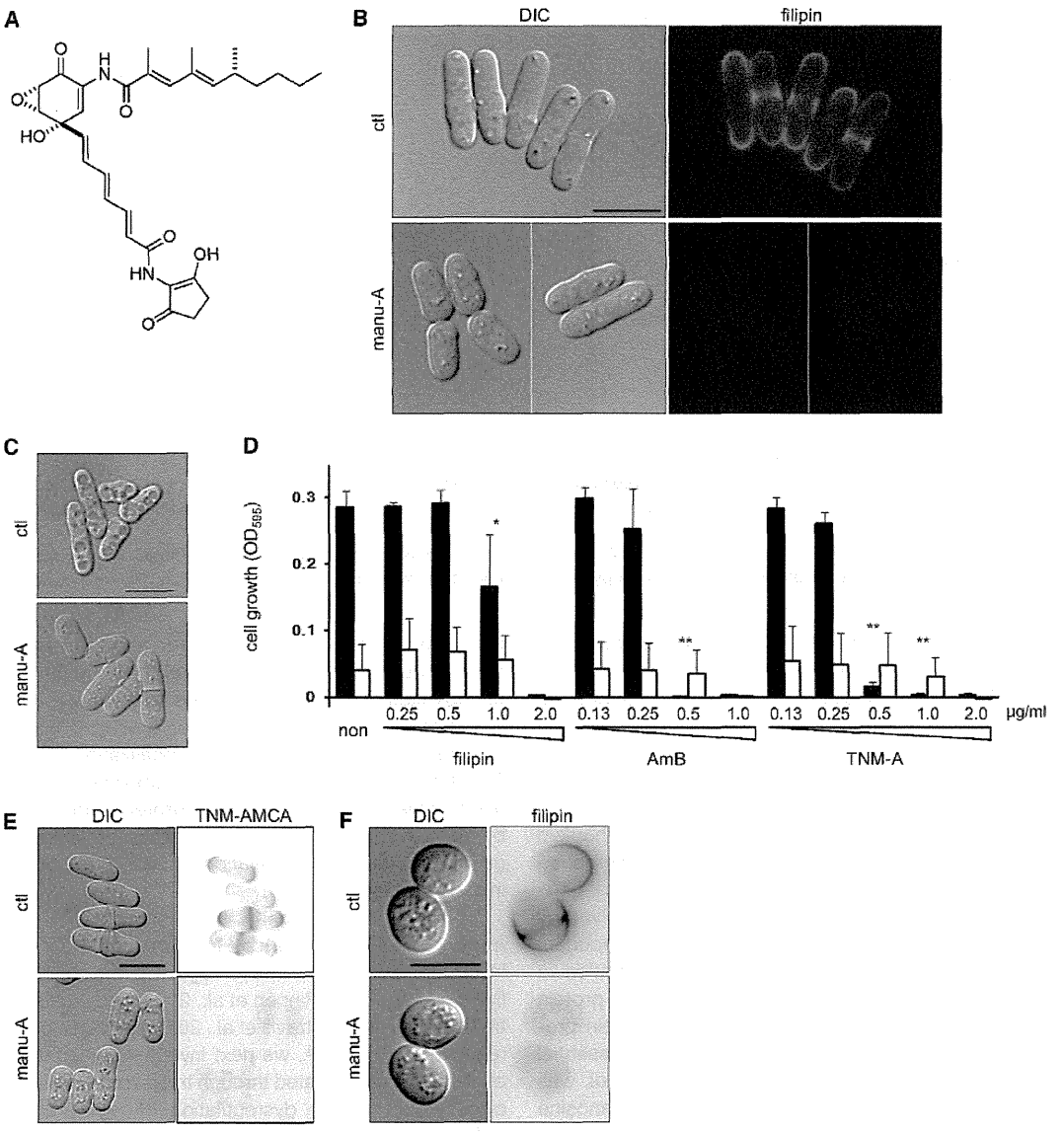

Figure 1. Manu-A Abolishment of the Binding and Effect of Sterol-Binding Antibiotics

(A) Chemical structure of manu-A.

(B) Sterol-rich plasma membrane domains of fission yeast cells. Domains were visualized with filipin (upper right hand panel). Manu-A treatment (1 μg/ml) for 1 hr abolished the fluorescent signal of filipin binding (lower right hand panel).

(C) Cellular effect of AmB. Cells were treated with AmB (1 μg/ml) for 1 hr in the presence or absence of manu-A (1 μg/ml) and observed under microscopy.

(D) Effect of manu-A on the growth inhibition exerted by antibiotics. Yeast cells were incubated with sterol-targeting antibiotics in the presence (white) or absence (black) of manu-A (0.5 μg/ml) for 26 hr. Data represent the mean ± SD, n = 3–4. Statistical significance of $p < 0.05$ (*) and $p < 0.01$ (**) were determined by t test, calculated using cell growth values normalized using optical density of the cultures in the absence of manu-A.

(E) Binding of TNM-AMCA in the presence of manu-A. Cells were incubated with or without manu-A (1 μg/ml) for 1 hr, and then stained with TNM-AMCA (1 μg/ml) for 1 hr.

(F) Sterol-rich domains in *cpp1*Δ cells. The domains were visualized with filipin in the presence or absence of manu-A (1 μg/ml). Scale bars, 10 μm. Control (ctl), differential interference contrast microscopy (DIC).

Relationship between Manu-A and Cdc42

Sterol localization is controlled in a cell cycle-dependent manner (Wachtler et al., 2003); we therefore hypothesized that the effect of manu-A on the plasma membrane would correlate with its cell growth inhibitory activity. To identify the genes involved in the action of manu-A, we conducted a genome-wide screen using a decreased abundance by mRNA perturbation (DAmP) strain collection of the budding yeast *Saccharomyces cerevisiae* (Breslow et al., 2008; Yan et al., 2008). DAmP acts by destabilizing mRNA transcripts through the integration of an

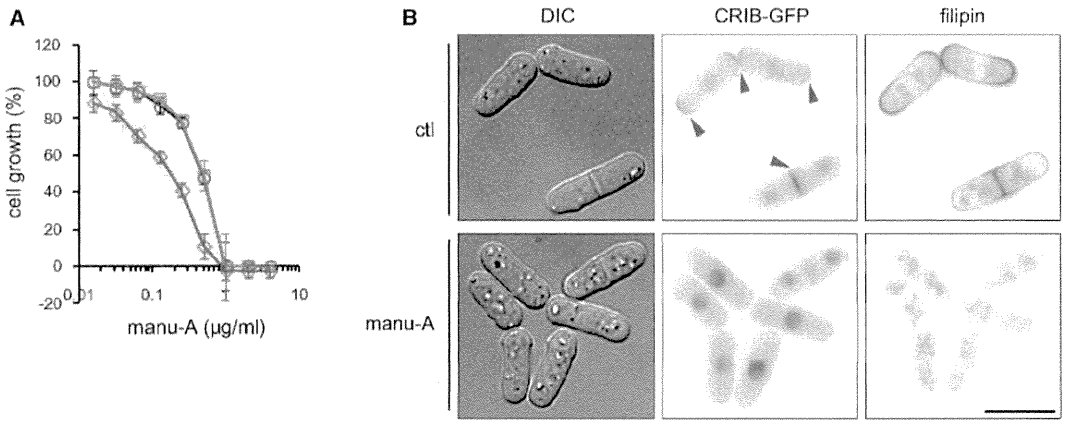

Figure 2. Relationship between Cdc42 and Manu-A

(A) Effect of Cdc42 expression levels on manu-A sensitivity. Cells containing mock vectors (black), cells overexpressing wild-type Cdc42 (blue), or the dominant-negative form, Cdc42-T17N (red), were cultured in the presence of manu-A. Cell growth was measured after 48 hr incubation. Data represent the mean ± SD, n = 4.

(B) Cellular localization of activated Cdc42 (detected using CRIB-GFP) and sterol-rich membrane domains (detected using filipin). Cells treated with or without manu-A (1 μg/ml) for 1 hr were observed under fluorescent microscopy. Arrowheads indicate the colocalization of CRIB-GFP and filipin signals. Scale bar, 10 μm.

antibiotic-selectable marker into the 3′ untranslated regions of genes of interest, thereby yielding hypomorphic alleles (Muhlrad and Parker, 1999). Genes involved in the mode of action of a bioactive compound can then be identified by screening DAmP strain collections for strains that are sensitive to the compound (Breslow et al., 2008; Yan et al., 2008).

The growth of the budding yeast cells was observed to be sensitive to manu-A (Figure S4A). After screening 878 haploid DAmP strains, we identified 28 genes for which downregulation conferred increased sensitivity to manu-A (Figures S4A–S4C). Among these, we found several genes involved in membrane trafficking: *SEC31*, which encodes a component of the COPII vesicle coat required for vesicle formation in ER-to-Golgi transport; and *PAN1*, which encodes a protein that associates with actin patches and promotes protein-protein interactions essential for endocytosis. *ERG8*, an essential gene for the biosynthesis of isoprenoids and ergosterol, was also identified. Notably, *CDC24*, which encodes a guanosine diphosphate-guanosine triphosphate (GTP) exchange factor for Cdc42, was similarly identified as a sensitive DAmP mutant (Park and Bi, 2007). Cdc42 is known to regulate the polarization of the actin cytoskeleton and membrane trafficking toward the sites of cell growth (Park and Bi, 2007; Perez and Rincón, 2010).

These results led us to hypothesize that manu-A perturbs Cdc42, which in turn effects the formation of sterol-rich membrane domains. To test whether manu-A targets the Cdc42 pathway in fission yeast, we first examined the effect of overexpression of Cdc42 on the growth inhibitory activity of manu-A. Overexpression of wild-type Cdc42 had no effect, whereas cells expressing the dominant-negative form of Cdc42 became more sensitive to manu-A compared with cells containing mock vectors (Figure 2A). We next examined the activity of Cdc42 using a fluorescent fusion protein called Cdc42/Rac interactive binding peptide-green fluorescent protein (CRIB)-GFP, which specifically binds to activated, GTP-bound Cdc42 (Tatebe et al., 2008). In wild-type cells, CRIB-GFP signal was concentrated at the growing cell tips during interphase and around the division plane during mitosis (Figure 2B). After the addition of manu-A, cortical GFP signal was barely detectable, indicating that Cdc42 was inactivated. In contrast, cortical localization visualized using GFP-Cdc42 fusion protein was not abolished completely, and the prenylation status of Cdc42 protein appeared unaffected by manu-A (Figures S4D and S4E). Together, these results suggested that the Cdc42 activation pathway is targeted by manu-A in fission yeast cells.

Inhibition of Exocytosis by Manu-A

In fission yeast cells, Cdc42 regulates the actin cytoskeleton (Martin et al., 2007; Rincón et al., 2009) and multiple membrane trafficking events (Estravís et al., 2011). Since Cdc42 was downregulated by manu-A, we next investigated whether the effect of manu-A was mediated through the disorganization of the actin cytoskeleton and/or dysregulation of membrane trafficking. In fission yeast cells, the actin cytoskeleton consists of actin cables, actin patches, and a contractile ring during vegetative growth (Kovar et al., 2011). Cells treated with manu-A exhibited apparently delocalized actin patches with randomly localized actin cables, indicating that cells lost polarity in actin structures in the presence of manu-A (Figure S5A). However, genetic perturbation of the actin cytoskeleton organization did not result in a similar phenotype; when temperature-sensitive *cps8-188* cells were left at the restriction temperature, the fluorescent signal of filipin became delocalized and distributed over the plasma membrane (Codlin et al., 2008). Furthermore, the effect of manu-A on cell growth was almost indistinguishable between actin mutant cells and wild-type cells (Figure 3A). These results indicated that the effect of manu-A on the plasma membrane was not exerted through disorganization of the actin cytoskeleton.

Next, we investigated the relationship between manu-A and membrane trafficking. A terminal phenotype of a thermosensitive

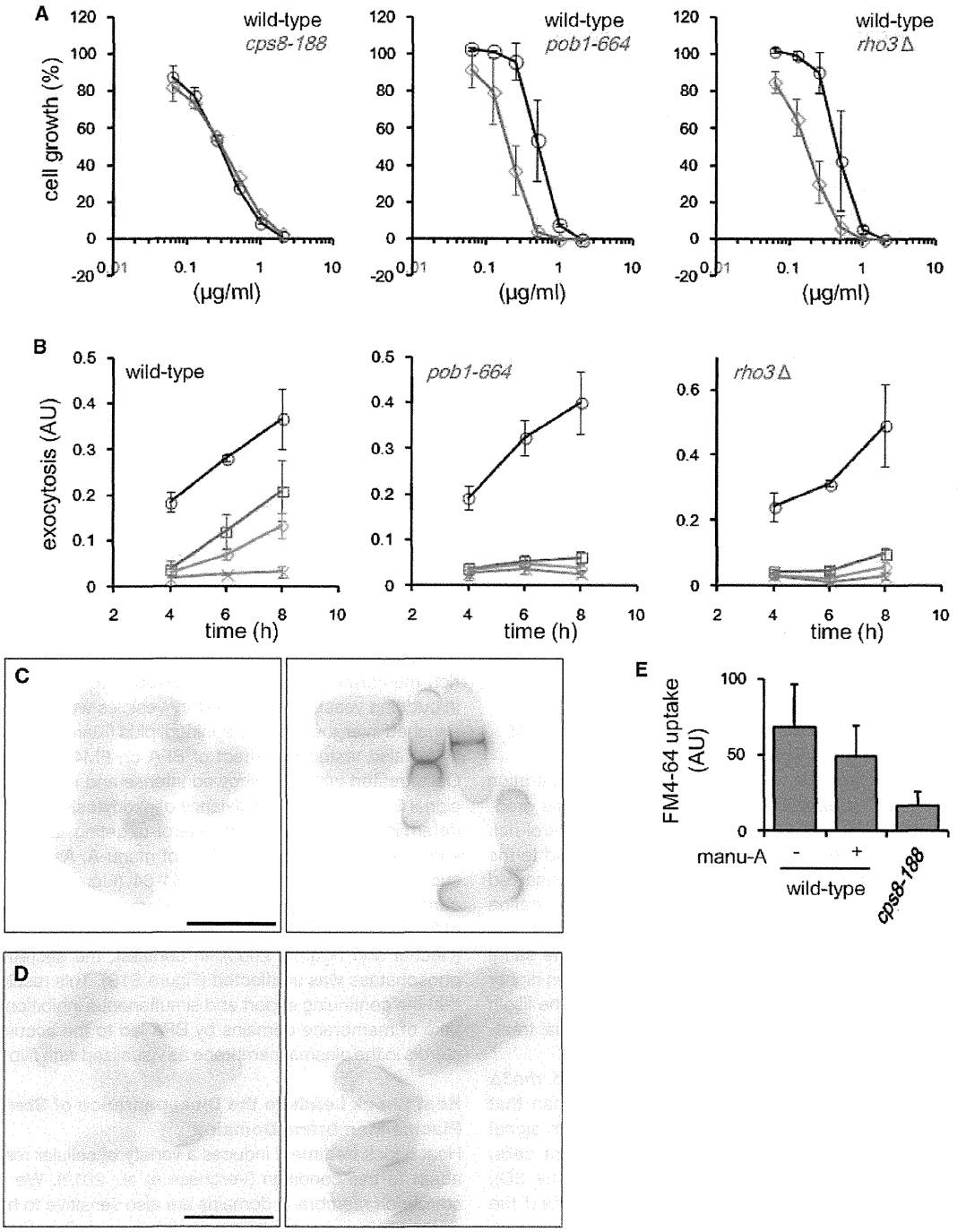

Figure 3. Effect of Manu-A on Cell Growth, Exocytosis, and Endocytosis

(A) Growth inhibition of mutant cells by manu-A. Growth of *cps8-188* cells (27°C for 24 hr), *pob1-664* cells (30°C for 26 hr), and *rho3*Δ cells (30°C for 26 hr) in the presence of manu-A was compared with that of wild-type cells.

(B) Exocytosis inhibition by manu-A. Activity of secreted acid phosphatase from wild-type, *pob1* mutant, and *rho3* deletion cells in the presence of manu-A was measured. Acid phosphatase activity was normalized with cell density. Cells were cultivated at 27°C and at various manu-A concentrations: 0 (black), 0.05 (red), 0.1 (blue), and 0.5 (green) μg/ml.

(C) Reappearance of sterol-rich membrane domains after treatment with a low concentration of manu-A. Manu-A (0.05 μg/ml) was added to the cells in EMMP, followed by visualization of sterol-rich membrane domains using filipin. Fluorescent images after 1 hr treatment (left) and 5 hr treatment (right) are shown.

(legend continued on next page)

strain of *cdc42* is a defect in exocytosis (Estravís et al., 2011). To test the possibility that manu-A inhibits exocytosis, we measured the secretion of acid phosphatase, a protein marker of exocytosis (Wang et al., 2002). When cells were exposed to manu-A, secretion of acid phosphatase was inhibited in a dose-dependent manner (Figure 3B). The effective concentration was comparable to that necessary for inhibiting the cellular binding of antibiotics. Many protein factors have been reported to be involved in exocytosis; for example, Pob1, which is involved in polarized growth; and a small GTPase, Rho3, which regulates cell separation. Although the precise molecular mechanism remains to be clarified, introducing mutations in the *pob1* gene (*pob1-664*; see Nakano et al., 2011) or deletion of the *rho3* gene (*rho3*Δ; see Wang et al., 2003) have been shown to decrease secretion resulting from exocytosis. When we challenged these mutant cells with manu-A, exocytosis was suppressed at lower manu-A concentrations compared with the wild-type cells (Figure 3B); moderate inhibition was observed in wild-type cells at 0.05–0.1 μg/ml, whereas exocytosis was almost completely inhibited in the mutant cells at a concentration as low as 0.05 μg/ml. Additionally, manu-A more efficiently inhibited cell growth of the exocytosis mutant cells compared with the wild-type cells (Figure 3A). In contrast, exocytosis of actin mutant cells was not more sensitive to manu-A compared with wild-type cells (Figure S5B). These results showed that the observed cell growth inhibition by manu-A was, at least in part, a result of the suppression of exocytosis, which in turn led to the loss of cellular binding of sterol-targeting antibiotics.

Inhibition of Exocytosis Leads to the Disappearance of Sterol-Rich Plasma Membrane Domains

Treatment of wild-type cells with manu-A at a low concentration (0.05 μg/ml) inhibited exocytosis, but this inhibition was gradually released (Figure 3B). If exocytosis supplies sterol-rich membrane domains, recovery of exocytosis should lead to the recovery of these membrane domains. We indeed observed this using filipin staining of cells treated with a low concentration of manu-A; although treating wild-type cells with 0.05 μg/ml manu-A for 1 hr initially abolished the filipin signal, the same signal reappeared 5 hr later (Figure 3C). In contrast, when higher concentrations of manu-A were used, e.g., 0.5 μg/ml, the filipin signal was only barely detectable 6 hr following the initial treatment (Figure S6).

The exocytosis activities of the *pob1* mutant and *rho3*Δ cells were found to be more sensitive to manu-A than that of wild-type cells. We examined recovery of the filipin signal in these mutant cells and found that in *pob1* mutant cells, recovery of the filipin signal was not observed (Figure 3D). Similarly, the lack of *rho3* protein significantly perturbed the signal recovery and only weak and irregular filipin staining was observed (Figure 3D). Together, these results indicate that manu-A inhibits exocytosis, the route by which the sterol-rich membrane domains are supplied to the plasma membrane.

Endocytosis Is Requisite for the Disappearance of Sterol-Rich Plasma Membrane Domains

Manu-A inhibits exocytosis, and this inhibition appears to abolish the production of sterol-rich membrane domains in the plasma membrane. However, inhibition of the supply of sterol-rich membrane domains may not to be sufficient for the complete abolishment of antibiotic action, since certain portions of the sterol-rich membrane domains should already have been delivered to the plasma membrane prior to the addition of manu-A. This suggested the possibility that endocytosis could selectively internalize these domains, a process that may not be inhibited by manu-A. Our next experiments therefore tested the effect of manu-A on endocytosis.

In fission yeast cells, the fluorescent styryl dye FM4-64 is used as a marker for the endocytic pathway, as FM4-64 is internalized by endocytosis at the growing areas of the cell and is subsequently transported to the vacuolar membrane (Gachet and Hyams, 2005). Within 30 min of the addition of FM4-64, intermediate compartments became stained despite the presence of manu-A (although the dye intensity was slightly decreased), indicating that endocytosis was uninhibited by manu-A (Figure 3E). This analysis suggested that manu-A did not inhibit the uptake of plasma membrane domains, despite inhibiting the supply thereof to the membrane and consequently inhibiting the generation of sterol-rich membrane domains. This corroborates a previous finding in budding yeast, where secretory vesicles were observed to be enriched in ergosterol and sphingolipids (Klemm et al., 2009).

We also tested the effect of BFA on FM4-64 incorporation. Cells treated with BFA showed intense and nonpolarized filipin signal (Figure S1A). If the balance of exocytosis and endocytosis determines the binding of sterol-targeting antibiotics, BFA should have the opposite effect of manu-A. As expected, BFA suppressed incorporation of FM4-64 (Figure S1C). This was consistent with a previous report demonstrating BFA inhibition of FM4-64 incorporation at the equatorial region in dividing cells (Gachet and Hyams, 2005). In contrast, the secretion of acid phosphatase was unaffected (Figure S1B). This result indicated that the continuing export and simultaneous inhibition of the uptake of membrane domains by BFA led to the accumulation of sterols in the plasma membrane as visualized with filipin staining.

Heat Shock Leads to the Disappearance of Sterol-Rich Plasma Membrane Domains

Heat shock treatment induces a variety of cellular responses to adapt to this condition (Verghese et al., 2012). We found that sterol-rich membrane domains are also sensitive to heat shock, as the filipin signal in wild-type cells was significantly decreased after the temperature was shifted from 27°C to 37°C (Figure 4A). This response was transient and the sterol-rich membrane

(D) Lack of reappearance of sterol-rich membrane domains in mutant cells. *pob1-664* (left) and *rho3*Δ cells (right) were treated with 0.05 μg/ml manu-A and stained with filipin after 5 hr.

(E) Effect of manu-A on endocytosis. Uptake of FM4-64 by wild-type cells was observed after treatment with DMSO (0.1%) or manu-A (1 μg/ml) for 1 hr. FM4-64 was added to the culture and cells were observed under fluorescence microscopy. Uptake of FM4-64 was calculated after 0.5 hr. In a control experiment, *cps8-188* cells were shifted to the restriction temperature (37°C) for 1 hr, followed by FM4-64 treatment and observation of FM4-64 uptake.

In (A) and (B), data represent the mean ± error bars, SD, n = 3. In (E), data represent the mean ± error bars, SE, n = 3.

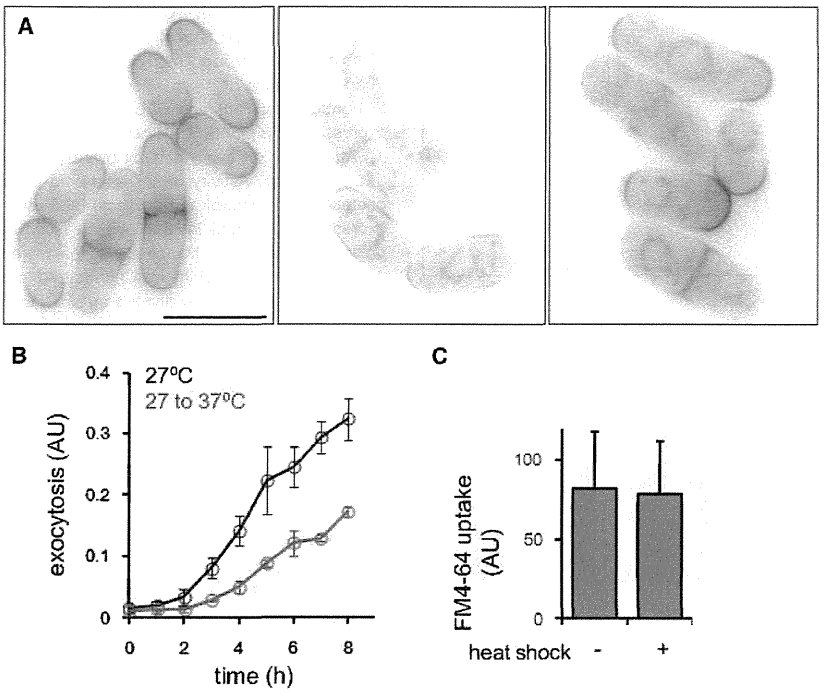

Figure 4. Transient Disappearance of Sterol-Rich Plasma Membrane Domains following Heat Shock

(A) Disappearance and reappearance of sterol-rich plasma membrane domains following heat shock treatment. Wild-type cells in YE5S were shifted from 27°C (left) to 37°C for 1 hr (middle) and 5 hr (right), and the presence of sterol-rich membrane domains was visualized using filipin. Scale bar, 10 μm.

(B) Kinetics of exocytosis after heat shock. Cells were cultured at 27°C (black) or shifted from 27°C to 37°C (red) at time 0. Activity of secreted acid phosphatase was measured and normalized with cell density. Data represent the mean ± SD, n = 3.

(C) Effect of heat shock on endocytosis. Wild-type cells in YE5S were shifted from 27°C (left) to 37°C for 1 hr, and uptake of FM4-64 was observed. Data represent the mean ± SE, n = 3.

domains gradually reappeared (Figure 4A). We hypothesized that this phenomena may be similar in mechanism to that of treatment with low concentrations of manu-A, and we expected that while heat shock may transiently suppress exocytosis, endocytosis would not be affected. To test this hypothesis, we analyzed the kinetics of exocytosis after heat shock (Figure 4B). As expected, exocytosis was attenuated and no release of acid phosphatase was observed 2 hr after the temperature shift. As a consequence, the concentration of released acid phosphatase was lower than that for the control cells (no temperature shift). In contrast, cellular uptake of FM4-64 was uninhibited by the temperature shift (Figure 4C). We therefore concluded that heat shock temporarily halts exocytosis, but not endocytosis, thereby facilitating the disappearance of sterol-rich membrane domains in the plasma membrane, similar in effect to manu-A treatment.

Sterol-Targeting Antibiotic-Resistant Cells Exhibit Defect in Exocytosis

Resistance to antibiotics can be the result of multiple mechanisms. Our emerging model suggested the possibility that cells may exhibit tolerance toward sterol-targeting antibiotics where a defect in exocytosis is present. To investigate this possibility, we first examined the secretion of acid phosphatase from ergosterol mutant cells. Knockout of the *erg2* gene or simultaneous deletion of the *erg31* and *erg32* genes in fission yeast is known to cause tolerance to sterol-targeting antibiotics (Iwaki et al., 2008). However, we could not detect any defects in acid phosphatase secretion (data not shown).

We next examined overexpression of the *SPCC23B6.04c* gene. We previously conducted genome-wide screening to identify genes conferring altered sensitivity to chemicals by their overexpression (Nishimura et al., 2010). Among the ~4,800 genes screened, *SPCC23B6.04c* was identified as a resistance gene common to AmB, nystatin, and TNM-F, a closely related congener of TNM-A (Matsunaga et al., 1989). We first investigated the cellular binding of filipin and TNM-AMCA to cells overexpressing *SPCC23B6.04c*. As expected, neither compound bound to the cells (Figures 5A and 5B), suggesting that antibiotic-sensitive sterol-rich membrane domains are not supplied to the plasma membrane in these cells. Next, we measured the degree of exocytosis and endocytosis. We found that the secretion of acid phosphatase was significantly decreased by overexpression of *SPCC23B6.04c* (Figure 5C). When overexpression was suppressed by addition of thiamine, this defect was not observed. In contrast, endocytosis was unaffected by overexpression of this gene (Figure 5D). The intensity of FM4-64 dye incorporated into these cells was no different to that of the control cells. Although the molecular function of the gene product of *SPCC23B6.04c* is still unknown, these results add further support to our model (discussed below, Figure 6).

Model for the Generation of Antibiotic-Sensitive Sterol-Rich Plasma Membrane Domains

Based on our results, we propose a model in which exocytosis supplies and endocytosis internalizes the specific membrane domains recognized by sterol-targeting antibiotics (Figure 6). In this study, we first showed that manu-A caused defects in membrane trafficking and abolishment of the effect of sterol-targeting antibiotics. Manu-A inhibited Cdc42 activity and its downstream event, exocytosis. In contrast, endocytosis was only partially inhibited. Heat shock and overexpression of a gene with unknown function, *SPCC23B6.04c*, induced similar defects in membrane trafficking and decreased binding of sterol-targeting antibiotics. BFA inhibited the incorporation of FM4-64, but not the secretion of acid phosphatase. Treatment with BFA exhibited intense fluorescence of filipin at the plasma membrane, suggesting that the selective inhibition of endocytosis resulted in the accumulation

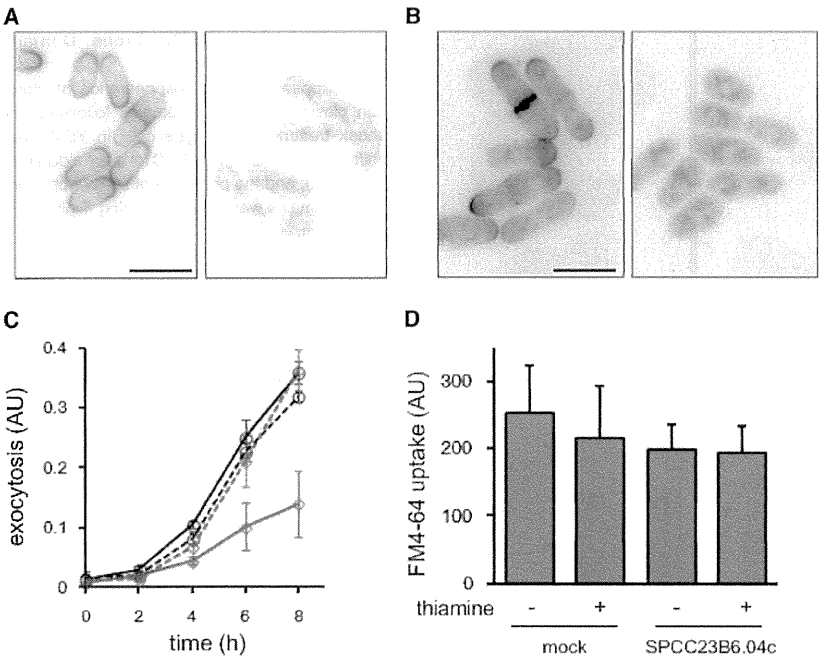

Figure 5. Effect of Overexpression of *SPCC23B6.04c* on Sterol-Targeting Antibiotics and Membrane Trafficking

(A and B) Binding of filipin (A) or TNM-AMCA (B) to control cells (left) and *SPCC23B6.04c*-overexpressing cells (right). Scale bars, 10 μm.

(C) Attenuation of exocytosis by overexpressing *SPCC23B6.04c*. Activity of secreted acid phosphatase from control cells (black) and overexpressing cells (red) in the absence (solid) or presence (dashed) of thiamine was measured. Acid phosphatase activity was normalized with cell density. Cells were cultivated at 27°C. Error bars, SD, n = 3.

(D) Effect of overexpression of *SPCC23B6.04c* on endocytosis. Uptake of FM4-64 by control and overexpressing cells was observed. Error bars, SE, n = 3.

of excess sterols. Taken together, balanced membrane trafficking appears essential for the regulation of the quantity of antibiotic-sensitive and sterol-rich domains in the plasma membrane.

SIGNIFICANCE

The species and quantity of lipid molecules in the plasma membrane are maintained by multiple mechanisms involving vesicle transport, lipid transport proteins, and local metabolic reactions (van Meer et al., 2008). Here, we have demonstrated that the proper balance between exocytosis and endocytosis produces membrane domains that are recognized by sterol-targeting antibiotics, as the specific inhibition of exocytosis, but not endocytosis by manu-A, heat shock, or overexpression of *SPCC23B6.04c*, all abolished the cellular binding of these antibiotics. Originally, membrane domains stainable by filipin were termed sterol-rich membrane domains (Wachtler et al., 2003), and similar staining patterns have since been observed when using fluorescently labeled TNMs (Nishimura et al., 2010). However, manu-A abolished the efficacy of not only filipin and TNMs, but also that of AmB, for which the subcellular localization remains unknown. Based on these observations, we suggest that the sterol-rich membrane domains are also intrinsically antibiotic-sensitive, at least in fission yeast. In silico simulations, based on experimental data, have predicted that the actin cytoskeleton, exocytosis, and endocytosis all coordinate to create cell polarity (Chou et al., 2012), which in turn is most likely regulated by Cdc42 (Mogilner et al., 2012). Many protein factors involved in cell polarization have been identified. However, mutations of these genes usually affect the total cell morphogenesis. Manu-A enables quick and complete inhibition of Cdc42 activity and exocytosis, leading to the disappearance of sterol-rich antibiotic-sensitive membrane domains without the loss of cell shape polarity. This microbial metabolite could therefore prove a valuable tool for investigating the molecular mechanisms underlying the establishment and maintenance of cell morphogenesis.

EXPERIMENTAL PROCEDURES

Reagents

Filipin and AmB were purchased from Sigma-Aldrich. FM4-64 was from Invitrogen. TNM-AMCA was prepared as described previously (Ho et al., 2009). Manu-A was a gift from Kyowa Hakko Kirin. Anti-GFP antibody (GF200) was purchased from Nacalai Tesque, and anti-α-tubulin antibody (B-5-1-2) was from Sigma-Aldrich.

Yeast Strains

Deletion of the *cpp1* gene (SN246: *h⁻ leu1-32 cpp1::kan*^{r}) and *rho3* gene (SN168: *h⁻ rho3::kan*^{r}), and overexpression and tagging of Cdc42 were carried out as described in the Supplemental Experimental Procedures. An overexpression strain, *SPCC23B6.04c*, was constructed as previously reported (Matsuyama et al., 2006). Overexpression was induced in the absence of thiamine, whereas promoter activity was suppressed by the addition of thiamine (5 μM). Other strains were gifts from various yeast researchers.

Microscopy

Cells were treated with compounds at 27°C unless stated otherwise in the figure legends. Staining with filipin and TNM-AMCA were carried out as previously described (Nishimura et al., 2010; Wachtler et al., 2003). Vacuole morphology was visualized with FM4-64 as previously described (Gachet and Hyams, 2005). A MetaMorph system (Molecular Devices) was used for image acquisition together with an Olympus IX81 fluorescence microscope equipped with an UPLSAPO 100 × lens. Fluorescence intensity was quantified using the MetaMorph software.

Extraction and Analysis of Sterols

Cells were cultivated in the presence or absence of manu-A, harvested, washed with ice-cold water, and stored at −80°C until extraction. Cells (~3×10^7) were suspended in 75% aqueous MeOH (2 ml) containing 0.1% pyrogallol and 10 μg 4,4′-di-tert-butyl-2,2′-bipyridiyl as an internal control. $CHCl_3$ (1 ml) was added to the suspension, which was then vortexed vigorously (30 s).

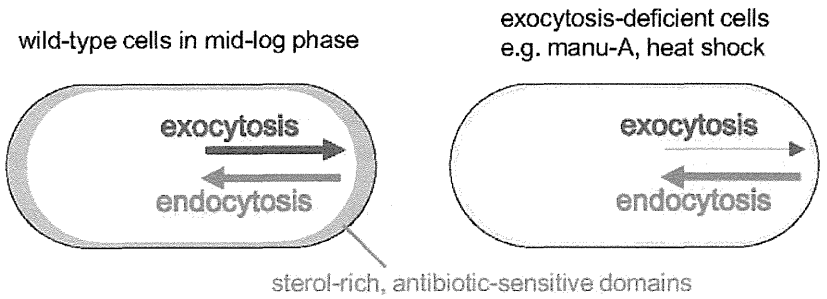

Figure 6. Model of the Production of Sterol-Rich/Antibiotic-Sensitive Plasma Membrane Domains

In actively dividing cells, exocytosis supplies sterol-rich and probably antibiotic-sensitive membrane domains to the plasma membrane. Endocytosis internalizes these domains. After the addition of manu-A or heat shock treatment, exocytosis is selectively suppressed while endocytosis is unaffected, leading to the disappearance of sterol-rich and antibiotic-sensitive membrane domains.

Petroleum ether (2 ml) was added to the mixture, followed by vortexing and centrifugation, and the upper layer was subsequently collected. This procedure was repeated twice to obtain three petroleum ether extracts. The extracts were pooled, dried over Na_2SO_4, and concentrated in vacuo. The pellet was dissolved in *N,N*-dimethylformamide (100 μl), and 2 μl of this suspension was analyzed by high performance liquid chromatography (HPLC). The HPLC conditions were as follows: column, Shiseido Capcell Pak C18 UG120 φ 4.6 × 250 at 40°C; solvent system, 85%–100% MeOH over 20 min followed by 100% MeOH for 10 min with a flow rate of 1 ml/min; and detection, 282 nm. The quantity of ergosterol detected was calculated and normalized using the internal control.

Measurement of Acid Phosphatase Secretion

Acid phosphatase secretion was assayed as described previously with some modifications (Nakano et al., 2011; Wang et al., 2002). Cells grown overnight in YE5S media at 27°C were then cultivated at 27°C overnight in Edinburgh minimal medium (EMM) media. Cells were pelleted, washed with EMM without phosphate (EMMP), and suspended in fresh EMMP. Cell cultures (at an OD_{595} of 0.2) were incubated at 27°C with or without manu-A. At each time point, 500 μl culture were centrifuged, and 400 μl of the subsequent supernatant were added to 400 μl substrate solution (2 mM *p*-nitrophenyl phosphate, 0.1 M sodium acetate, pH 4.0; prewarmed to 30°C), and the mixture was then incubated at 30°C for 5 min. Reactions were stopped by the addition of 400 μl of 1 M NaOH. The absorbance at 405 nm was measured using the medium only as a blank control, and exocytosis efficiency was calculated as the ratio of OD_{405}/OD_{595}.

Statistical Analysis

Results are shown as mean values ± SD or SE as indicated in the figure legends. Statistical significance was determined by Student's t test.

SUPPLEMENTAL INFORMATION

Supplemental Information includes Supplemental Experimental Procedures and six figures and can be found with this article online at http://dx.doi.org/10.1016/j.chembiol.2014.10.014.

ACKNOWLEDGMENTS

We thank Kyowa Hakko Kirin for the kind gift of manu-A. We are grateful to J. Ishiguro (Konan University) for the *act1/cps8* mutant strain and M. Yamamoto (The University of Tokyo) for the *pob1* mutant strain, both of which were provided through the Yeast Genetic Resource Center. We also thank R. Sugiura (Kinki University) for the *cpp1* mutant strain, H. Tatebe and K. Shiozaki (Nara Institute of Science and Technology) for the CRIB-expressing strain, M. Balasubramanian (Temasek Life Sciences Laboratory) for the lifeact-expressing strain, P. Pérez (Universidad de Salamanca) for the *cwg2* mutant strain, K.L. Gould (Vanderbilt University School of Medicine) for the *css1* mutant strain, and K. Takegawa (Kyushu University) for the ergosterol mutant strains. This work was supported in part by a Grant-in-Aid from the Japan Society for the Promotion of Science and the Ministry of Education, Culture, Sports, Science, and Technology of Japan.

Received: February 14, 2014
Revised: September 26, 2014
Accepted: October 30, 2014
Published: December 11, 2014

REFERENCES

Arenz, C., Thutewohl, M., Block, O., Waldmann, H., Altenbach, H.J., and Giannis, A. (2001). Manumycin A and its analogues are irreversible inhibitors of neutral sphingomyelinase. ChemBioChem *2*, 141–143.

Bhuiyan, M.S., Ito, Y., Nakamura, A., Tanaka, N., Fujita, K., Fukui, H., and Takegawa, K. (1999). Nystatin effects on vacuolar function in Saccharomyces cerevisiae. Biosci. Biotechnol. Biochem. *63*, 1075–1082.

Bolard, J. (1986). How do the polyene macrolide antibiotics affect the cellular membrane properties? Biochim. Biophys. Acta *864*, 257–304.

Breslow, D.K., Cameron, D.M., Collins, S.R., Schuldiner, M., Stewart-Ornstein, J., Newman, H.W., Braun, S., Madhani, H.D., Krogan, N.J., and Weissman, J.S. (2008). A comprehensive strategy enabling high-resolution functional analysis of the yeast genome. Nat. Methods *5*, 711–718.

Chou, C.S., Moore, T.I., Chang, S.D., Nie, Q., and Yi, T.M. (2012). Signaling regulated endocytosis and exocytosis lead to mating pheromone concentration dependent morphologies in yeast. FEBS Lett. *586*, 4208–4214.

Codlin, S., Haines, R.L., and Mole, S.E. (2008). btn1 affects endocytosis, polarization of sterol-rich membrane domains and polarized growth in *Schizosaccharomyces pombe*. Traffic *9*, 936–950.

Drabikowski, W., Lagwińska, E., and Sarzala, M.G. (1973). Filipin as a fluorescent probe for the location of cholesterol in the membranes of fragmented sarcoplasmic reticulum. Biochim. Biophys. Acta *291*, 61–70.

Espiritu, R.A., Matsumori, N., Murata, M., Nishimura, S., Kakeya, H., Matsunaga, S., and Yoshida, M. (2013). Interaction between the marine sponge cyclic peptide theonellamide A and sterols in lipid bilayers as viewed by surface plasmon resonance and solid state H NMR. Biochemistry *52*, 2410–2418.

Estravís, M., Rincón, S.A., Santos, B., and Pérez, P. (2011). Cdc42 regulates multiple membrane traffic events in fission yeast. Traffic *12*, 1744–1758.

Fang, Y., Hu, L., Zhou, X., Jaiseng, W., Zhang, B., Takami, T., and Kuno, T. (2012). A genomewide screen in Schizosaccharomyces pombe for genes affecting the sensitivity of antifungal drugs that target ergosterol biosynthesis. Antimicrob. Agents Chemother. *56*, 1949–1959.

Gachet, Y., and Hyams, J.S. (2005). Endocytosis in fission yeast is spatially associated with the actin cytoskeleton during polarised cell growth and cytokinesis. J. Cell Sci. *118*, 4231–4242.

Graham, T.R., Scott, P.A., and Emr, S.D. (1993). Brefeldin A reversibly blocks early but not late protein transport steps in the yeast secretory pathway. EMBO J. *12*, 869–877.

Gray, K.C., Palacios, D.S., Dailey, I., Endo, M.M., Uno, B.E., Wilcock, B.C., and Burke, M.D. (2012). Amphotericin primarily kills yeast by simply binding ergosterol. Proc. Natl. Acad. Sci. USA *109*, 2234–2239.

Hara, M., Akasaka, K., Akinaga, S., Okabe, M., Nakano, H., Gomez, R., Wood, D., Uh, M., and Tamanoi, F. (1993). Identification of Ras farnesyltransferase inhibitors by microbial screening. Proc. Natl. Acad. Sci. USA *90*, 2281–2285.

Hayles, J., and Nurse, P. (2001). A journey into space. Nat. Rev. Mol. Cell Biol. *2*, 647–656.

Ho, C.H., Magtanong, L., Barker, S.L., Gresham, D., Nishimura, S., Natarajan, P., Koh, J.L., Porter, J., Gray, C.A., Andersen, R.J., et al. (2009). A molecular barcoded yeast ORF library enables mode-of-action analysis of bioactive compounds. Nat. Biotechnol. *27*, 369–377.

Iwaki, T., Iefuji, H., Hiraga, Y., Hosomi, A., Morita, T., Giga-Hama, Y., and Takegawa, K. (2008). Multiple functions of ergosterol in the fission yeast *Schizosaccharomyces pombe*. Microbiology *154*, 830–841.

Klemm, R.W., Ejsing, C.S., Surma, M.A., Kaiser, H.J., Gerl, M.J., Sampaio, J.L., de Robillard, Q., Ferguson, C., Proszynski, T.J., Shevchenko, A., and Simons, K. (2009). Segregation of sphingolipids and sterols during formation of secretory vesicles at the trans-Golgi network. J. Cell Biol. *185*, 601–612.

Kovar, D.R., Sirotkin, V., and Lord, M. (2011). Three's company: the fission yeast actin cytoskeleton. Trends Cell Biol. *21*, 177–187.

Ma, Y., Kuno, T., Kita, A., Asayama, Y., and Sugiura, R. (2006). Rho2 is a target of the farnesyltransferase Cpp1 and acts upstream of Pmk1 mitogen-activated protein kinase signaling in fission yeast. Mol. Biol. Cell *17*, 5028–5037.

Martin, S.G., Rincón, S.A., Basu, R., Pérez, P., and Chang, F. (2007). Regulation of the formin for3p by cdc42p and bud6p. Mol. Biol. Cell *18*, 4155–4167.

Matsunaga, S., and Fusetani, N. (1995). Theonellamides A-E, cytotoxic bicyclic peptides, from a marine sponge *Theonella* sp. J. Org. Chem. *60*, 1177–1181.

Matsunaga, S., Fusetani, N., Hashimoto, K., and Walchli, M. (1989). Bioactive marine metabolites 0.26. Theonellamide F - a novel antifungal bicyclic peptide from a marine sponge *Theonella sp*. J. Am. Chem. Soc. *111*, 2582–2588.

Matsuyama, A., Arai, R., Yashiroda, Y., Shirai, A., Kamata, A., Sekido, S., Kobayashi, Y., Hashimoto, A., Hamamoto, M., Hiraoka, Y., et al. (2006). ORFeome cloning and global analysis of protein localization in the fission yeast Schizosaccharomyces pombe. Nat. Biotechnol. *24*, 841–847.

Mogilner, A., Allard, J., and Wollman, R. (2012). Cell polarity: quantitative modeling as a tool in cell biology. Science *336*, 175–179.

Muhlrad, D., and Parker, R. (1999). Aberrant mRNAs with extended 3′ UTRs are substrates for rapid degradation by mRNA surveillance. RNA *5*, 1299–1307.

Nakano, K., Toya, M., Yoneda, A., Asami, Y., Yamashita, A., Kamasawa, N., Osumi, M., and Yamamoto, M. (2011). Pob1 ensures cylindrical cell shape by coupling two distinct rho signaling events during secretory vesicle targeting. Traffic *12*, 726–739.

Nishimura, S., Arita, Y., Honda, M., Iwamoto, K., Matsuyama, A., Shirai, A., Kawasaki, H., Kakeya, H., Kobayashi, T., Matsunaga, S., and Yoshida, M. (2010). Marine antifungal theonellamides target 3β-hydroxysterol to activate Rho1 signaling. Nat. Chem. Biol. *6*, 519–526.

Nishimura, S., Ishii, K., Iwamoto, K., Arita, Y., Matsunaga, S., Ohno-Iwashita, Y., Sato, S.B., Kakeya, H., Kobayashi, T., and Yoshida, M. (2013). Visualization of sterol-rich membrane domains with fluorescently-labeled theonellamides. PLoS ONE *8*, e83716.

Park, H.O., and Bi, E. (2007). Central roles of small GTPases in the development of cell polarity in yeast and beyond. Microbiol. Mol. Biol. Rev. *71*, 48–96.

Perez, P., and Rincón, S.A. (2010). Rho GTPases: regulation of cell polarity and growth in yeasts. Biochem. J. *426*, 243–253.

Rincón, S.A., Ye, Y., Villar-Tajadura, M.A., Santos, B., Martin, S.G., and Pérez, P. (2009). Pob1 participates in the Cdc42 regulation of fission yeast actin cytoskeleton. Mol. Biol. Cell *20*, 4390–4399.

Simons, K., and Ikonen, E. (1997). Functional rafts in cell membranes. Nature *387*, 569–572.

Takeda, T., and Chang, F. (2005). Role of fission yeast myosin I in organization of sterol-rich membrane domains. Curr. Biol. *15*, 1331–1336.

Takeda, T., Kawate, T., and Chang, F. (2004). Organization of a sterol-rich membrane domain by cdc15p during cytokinesis in fission yeast. Nat. Cell Biol. *6*, 1142–1144.

Tanaka, T., Tsukuda, E., Uosaki, Y., and Matsuda, Y. (1996). EI-1511-3, -5 and EI-1625-2, novel interleukin-1 beta converting enzyme inhibitors produced by Streptomyces sp. E-1511 and E-1625. III. Biochemical properties of EI-1511-3, -5 and EI-1625-2. J. Antibiot. (Tokyo) *49*, 1085–1090.

Tatebe, H., Nakano, K., Maximo, R., and Shiozaki, K. (2008). Pom1 DYRK regulates localization of the Rga4 GAP to ensure bipolar activation of Cdc42 in fission yeast. Curr. Biol. *18*, 322–330.

Trajkovic, K., Hsu, C., Chiantia, S., Rajendran, L., Wenzel, D., Wieland, F., Schwille, P., Brügger, B., and Simons, M. (2008). Ceramide triggers budding of exosome vesicles into multivesicular endosomes. Science *319*, 1244–1247.

van Meer, G., Voelker, D.R., and Feigenson, G.W. (2008). Membrane lipids: where they are and how they behave. Nat. Rev. Mol. Cell Biol. *9*, 112–124.

Verghese, J., Abrams, J., Wang, Y., and Morano, K.A. (2012). Biology of the heat shock response and protein chaperones: budding yeast (Saccharomyces cerevisiae) as a model system. Microbiol. Mol. Biol. Rev. *76*, 115–158.

Volmer, A.A., Szpilman, A.M., and Carreira, E.M. (2010). Synthesis and biological evaluation of amphotericin B derivatives. Nat. Prod. Rep. *27*, 1329–1349.

Wachtler, V., Rajagopalan, S., and Balasubramanian, M.K. (2003). Sterol-rich plasma membrane domains in the fission yeast Schizosaccharomyces pombe. J. Cell Sci. *116*, 867–874.

Wang, H., Tang, X., Liu, J., Trautmann, S., Balasundaram, D., McCollum, D., and Balasubramanian, M.K. (2002). The multiprotein exocyst complex is essential for cell separation in *Schizosaccharomyces pombe*. Mol. Biol. Cell *13*, 515–529.

Wang, H., Tang, X., and Balasubramanian, M.K. (2003). Rho3p regulates cell separation by modulating exocyst function in *Schizosaccharomyces pombe*. Genetics *164*, 1323–1331.

Yan, Z., Costanzo, M., Heisler, L.E., Paw, J., Kaper, F., Andrews, B.J., Boone, C., Giaever, G., and Nislow, C. (2008). Yeast Barcoders: a chemogenomic application of a universal donor-strain collection carrying bar-code identifiers. Nat. Methods *5*, 719–725.

Yang, W., Urano, J., and Tamanoi, F. (2000). Protein farnesylation is critical for maintaining normal cell morphology and canavanine resistance in Schizosaccharomyces pombe. J. Biol. Chem. *275*, 429–438.

Zeeck, A., Schröder, K., Frobel, K., Grote, R., and Thiericke, R. (1987). The structure of manumycin. I. Characterization, structure elucidation and biological activity. J. Antibiot. *40*, 1530–1540.

Chemoradiation provides a physiological selective pressure that increases the expansion of aberrant *TP53* tumor variants in residual rectal cancerous regions

Kazuko Sakai[1], Shinsuke Kazama[2], Yuzo Nagai[2], Koji Murono[2], Toshiaki Tanaka[2], Soichiro Ishihara[2], Eiji Sunami[2], Shuta Tomida[1], Kazuto Nishio[1], Toshiaki Watanabe[2]

[1]Department of Genome Biology, Kinki University Faculty of Medicine, Osaka-Sayama, Osaka, 589-8511, Japan

[2]Department of Surgical Oncology, The University of Tokyo, Bunkyo-ku, Tokyo, 113-8655, Japan

Correspondence to:

Kazuto Nishio, **e-mail:** knishio@med.kindai.ac.jp

Toshiaki Watanabe, **e-mail:** watanabe-1su@h.u-tokyo.ac.jp

Keywords: Chemoradiation, Rectal cancer, *TP53*, deep sequencing, RNA sequencing

Received: July 06, 2014 ***Accepted:*** September 03, 2014 ***Published:*** October 07, 2014

ABSTRACT

Neoadjuvant chemoradiotherapy has been introduced in patients with surgically resected rectal cancer and reduced the local recurrence. Heterogeneity exists in rectal cancer, and we hypothesized that there are subclones resistant to chemoradiotherapy within the cancer mass.

We performed DNA-targeted sequencing of pre- and post-treatment tumor tissues obtained from 20 rectal cancer patients who received chemoradiotherapy. The variant frequency of the mutant clones was compared between pre- and post-treatment samples of nine non-responder patients. RNA-targeted sequencing of 57 genes related to sensitivity to chemotherapy and radiotherapy was performed for the paired samples. Immunohistochemical analyses of p53 expression were also performed on the paired samples from the nine non-responder patients.

DNA-sequencing detected frequent mutations of suppressor genes including *TP53*, *APC* and *FBXW7* in the post-treatment samples of the nine non-responders. The frequency of *TP53* mutations showed significant increases after chemoradiotherapy. RNA-targeted sequencing of 29 tumor tissues demonstrated that decreased expression of three genes and increased expression of four genes were detected in the post-treatment samples. Significantly increased expression of *TP53* was observed in the post-treatment samples. Immunohistochemical staining for p53 revealed that increased p53 intensity scores were observed after chemoradiotherapy. These results suggest that the tumors with *TP53* mutations tend to accumulate through chemoradiotherapy.

INTRODUCTION

Approximately 1.2 million people are diagnosed with colorectal cancer (CRC) each year, and ~600,000 people die from the disease worldwide [1]. Surgical treatment is performed to cure the disease, however, various types of recurrence develop after surgery. Among these, local recurrence is observed more frequently in rectal cancer than colon cancer patients, and frequently impairs the patient's quality of life [2, 3]. Therefore, pre-operative chemoradiotherapy has been introduced as neoadjuvant therapy in the treatment of rectal cancer in order to reduce the local recurrence rate [4, 5]. However, patients with rectal cancer exhibit a wide spectrum of responses to chemoradiotherapy. About 10% of the patients who receive chemoradiotherapy achieve a pathological complete responses (pCR), while one-third die within five years [2, 3]. It is important to increase the efficacy

of chemoradiotherapy and improve patient outcomes. Antimetabolite is a major chemotherapeutic agent used in combination with radiotherapy. However, other new agents have also been active when used in combination with radiotherapy for patients with rectal cancer. The clinical question remains, which chemotherapeutic would be best for use in combination with radiotherapy. Deep sequencing might give us the answer to this question. Therefore, the biomarkers predicting the sensitivity of chemoradiotherapy are clinically important.

Microarrays have been used extensively to identify differential gene expression profiles in many cancers, which has aided in the screening, prognosis and classification of tumors. There have been a few previous studies that have reported a signature of gene expression classifying the sensitivity of the particular tumor to chemoradiotherapy [6, 7]. However, microarrays have limitations, including their low sensitivity [8, 9], low dynamic range and the possible presence of hybridization artifacts [10]. In addition, relatively large amounts of frozen tumor tissue samples are necessary for this technology.

Recent cancer profiling studies have focused on next-generation sequencing (NGS) [11]. RNA sequencing of the steady-state RNA expression avoids the limitations of microarray expression and allows for massive parallel sequencing of millions of sequences on chips containing complementary DNA (cDNA) libraries, generating a higher number of transcript sequences than is possible by a microarray analysis [12]. Thus, RNA sequencing presents unprecedented possibilities for genomic characterization, and has significantly advanced our understanding of genomic organization, including allele-specific expression, novel transcripts and variant isoforms. The advantages of RNA sequencing include its large dynamic range, high sensitivity and rapid sequencing for the differential expression analysis [12].

It has often been discussed that the expression data for more than 20,000 genes is associated with high redundancy, and a large sample size is necessary for this type of validation. Therefore, in this study, we aimed to analyze the gene expression profiles of 57 selected genes. This gene set was selected based on the biological evidence of the chemosensitivity of tumors to antimetabolites and platinum agents, and the radiosensitivity of tumors (Supplementary Table 1). Some of the oncogene and suppressor genes were selected because these genes were reported to be related with sensitivity to cytotoxic chemotherapy and radiotherapy. In addition, family of topoisomerases (TOP1, TOP2A, and TOP2B) and uridine diphosphate (UDP)-glucuronosyl transferase 1A1 (UGT1A1) were included into the set because the topoisomerase inhibitor CPT-11 might be used for chemoradiotherapy. Tubulin beta 3 (TUBB3) and vascular endothelial growth factor (VEGFA) were included as possible markers for antimitotic agents and anti-angiogenesis inhibitors. NGS is also a widely-used technology for the gene analysis. However, the use of targeted RNA sequencing using the NGS technology has been limited for clinical formalin-fixed paraffin-embedded (FFPE) samples. In this study, we set up a multiple gene expression analysis for FFPE samples using targeted RNA sequencing (Ion-PGM, Life Technologies, Carlsbad, CA).

The development of CRC is a multistep process that involves the accumulation of a wide range of genetic and phenotypic alterations, leading to the aberrant expression of genes that regulate cell proliferation. Therefore, somatic mutations are often detected in CRC, and these mutations are part of key mechanisms resulting in carcinogenesis. Somatic mutations of cancer-related genes are also related to the chemoradiosensitivity and resistance of solid tumors. For example, the *KRAS* mutation status is related to chemoradioresistance [13], as well as treatment with anti-EGFR antibodies [14]. However, there have been no previous studies comparing the mutation profiles of the tumors and the pre- and post-treatment chemoradiosensitivity.

TP53 is an integral part of the DNA damage-induced apoptosis pathway, and mutations and overexpression of *TP53* are frequently observed in rectal cancer. Regions of low oxygen and necrosis are common features of solid tumors. We hypothesized that chemoradiation provides a physiological selective pressure on tumors that induces the expansion of variant cells, leading to the acquisition of *TP53* mutations. To test this hypothesis, we performed targeted sequencing for clinical FFPE specimens obtained from rectal cancer patients, and we tried to compare the mutation profiles of the tumor samples pre- and post-treatment, focusing on the *TP53* tumor-suppressor gene.

RESULTS

Somatic mutation profiling by targeted DNA sequencing

Among the 20 patients, 10 were classified as responders and 10 as non-responders, according to the histopathological examination. After chemoradiotherapy, responders and non-responders represented with pathological grade 2 and 1a, respectively (Supplementary Table 2). Median disease-free survival (DFS) and overall survival (OS) of total patients were 61.4 and 71.4 months, respectively (Supplementary Figure 1A). These are comparable to that in our previous reports [15]. In comparing DFS and OS between responder and non-responder group, median DFS (69.7 versus 55.9 months, $P = 0.0560$) and OS (79.9 versus 62.8 months, $P = 0.0263$) were longer in responders than non-responders (Supplementary Figure 1B and 1C). Somatic mutation profiling was performed by the targeted DNA sequencing of 50 cancer-related genes in the paired pre- and post-treatment samples from nine of the

non-responders, because a sufficient amount of tumor cells were not obtained in the post-treatment tissues in one case (No. 8). Among the post-treatment samples of these nine non-responders, we detected *TP53* mutations in eight cases (89%), *APC* mutations in three cases (33%), *FBXW7* mutations in three cases (33%), and *STK11*, *KIT* and *BRAF* mutations in one case each (11%). The frequency of corresponding mutations in the pre-treatment samples was analyzed. When comparing the pre- and post-treatment samples in each pair, we found that there was an increased frequency of mutants of the tumor suppressor genes in the post-treatment samples (Figure 1A). The frequency of *TP53* mutations tended to increase in the post-treatment samples compared to the pre-treatment samples ($P = 0.0752$, by a paired t-test, Figure 1B and Table 1). This result led us to surmise that the accumulation of mutations of tumor suppressor genes may be increased by chemoradiotherapy.

Changes in gene expression before and after chemoradiotherapy, as determined by RNA sequencing

We also performed targeted RNA sequencing on 29 clinical FFPE samples (including nine paired non-responder samples, 1 pre-treatment non-responder sample and 10 pre-treatment responder samples) obtained from the rectal cancer patients. Twenty nanogram RNA samples were subjected to a gene expression analysis by RNA sequencing for the 57 targeted genes. The median coverage of each sample ranged from six to 4019. Two post-treatment samples (Nos. 9 and 19) showed extremely low median coverage (six and 28, respectively), and these were filtered out from the further analysis. The geometric mean was calculated and used for normalization. The levels of expression of each gene in the responder and non-responder groups were

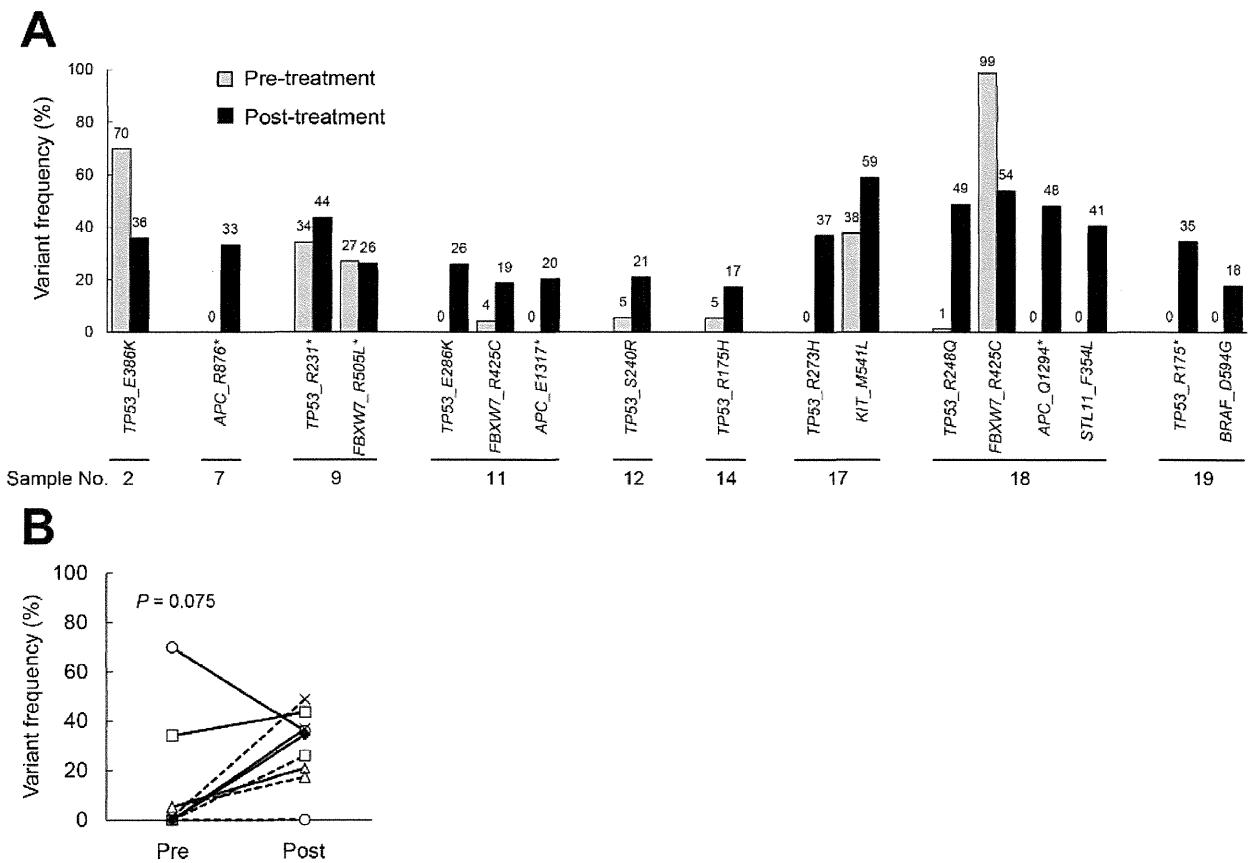

Figure 1: The frequency of gene mutations in samples obtained pre- and post-chemoradiation. The gene mutation status was evaluated by DNA sequencing, and the frequencies were compared between paired pre- and post-treatment samples from nine non-responders. **(A).** The mutation frequency in the pre- and post-chemoradiotherapy tumors. **(B).** The changes in the frequency of *TP53* mutations in the pre- and post-chemoradiation samples. Paired t-tests were used for the statistical analysis.

Table 1.

ID	*TP53* mutation site	*TP53* mutant frequency (%)		*TP53* relative gene expression		p53 IHC scoring index	
		pre	post	pre	post	pre	post
2	*TP53_E386K*	69.9	35.9	5776	6105	70	160
7	no *TP53* mutation	-	-	4182	2445	100	100
8	n.t.	n.t.	n.t.	n.t.	n.t.	n.t.	n.t.
9	*TP53_R231**	34.2	43.6	764	n.d.	0	50
11	*TP53_E286K*	0	25.9	0	8926	75	160
12	*TP53_S240R*	5.37	20.9	3482	7052	75	75
14	*TP53_R175H*	5.26	17.3	1878	7879	70	100
17	*TP53_R273H*	0	36.8	4314	10663	160	160
18	*TP53_R248Q*	1.26	48.8	1776	9247	140	180
19	*TP53_R175H*	0	34.5	5802	n.d.	55	180

n.t., a sufficient amount of tumor cells were not obtained in the post-treatment tissues; n.d., not detected.

plotted (Supplementary Figure 2). A non-parametric statistical method (Mann-Whitney U-test) was used for comparisons between the responders and non-responders.

The expression of *ABCG2* ($P = 0.0196$) and *TYMP* ($P = 0.0343$) was decreased in non-responders compared with responders. In contrast, increased expression of *NRP1* ($P = 0.0343$), *RPN2* ($P = 0.0233$), *TOP1* ($P = 0.0413$) and *TYMS* ($P = 0.0343$) was observed in non-responders compared with responders. The expression of tumor suppressor genes, including *TP53*, *PTEN* and *STK11*, was not significantly different between the two groups.

Next, the changes in gene expression between pre- and post-treatment samples in the non-responder group were plotted (Supplementary Figure 3). A paired t-test was used for comparisons between these pre- and post-treatment samples. Increased expression of *ABCG2* ($P = 0.0196$), *GSTP1* ($P = 0.0177$), *HMGB2* ($P = 0.0259$), *STMN1* ($P = 0.0006$), *TP53* ($P = 0.0241$), *TUBB3* ($P = 0.0226$) and *TYMP* ($P = 0.0022$) was observed in the post-treatment samples compared to the pre-treatment samples. In contrast, decreased expression of *DPYD* ($P = 0.0181$), *ERCC3* ($P = 0.0056$), *RPN2* ($P = 0.0105$), *RPM1* ($P = 0.0453$) and *TOP1* ($P = 0.0447$) was detected in the post-treatment samples.

To evaluate our hypothesis, we focused on the gene expression changes in tumor suppressor genes (*TP53*, *PTEN*, and *STK11*) between the pre- and post-treatment samples. Increased expression of *TP53* was observed in the post-treatment samples ($P = 0.024$, Figure 2, Table 1, and Supplementary Table 3).

Immunohistochemical staining of the p53 protein

To confirm our hypothesis, we performed immunohistochemical staining of p53 (the protein encoded by *TP53*) in paired samples using anti-p53 antibodies. Only nine samples were evaluable because there was no tumor tissue in one case. Increased p53 staining, as determined by the Intensity Score (area x intensity) for p53, was observed in six of the 9 post-treatment samples, and no change was observed in the other three samples (Figure 3, Table 1, and Supplementary Table 4). It is well known that overexpression of the p53 protein sometimes accompanies *TP53* mutation status (loss of function) [16]. Therefore, our results are consistent with the results of the DNA sequencing, and suggest that enrichment of tumor clones with alterations in tumor suppressor genes occurred during or after the chemoradiotherapy.

DISCUSSION

In this report, the frequency of *TP53* mutations was significantly enriched in the post-treatment samples compared to the pre-treatment samples. It is well known that colon cancer exhibits high heterogeneity. It can therefore be speculated that *TP53* mutation-positive tumor cells are present in most tumors. Mutations in *TP53* occur in half of all human cancers [17], indicating its critical importance in inhibiting cancer development. *TP53* is involved in apoptosis, the response to DNA damage and

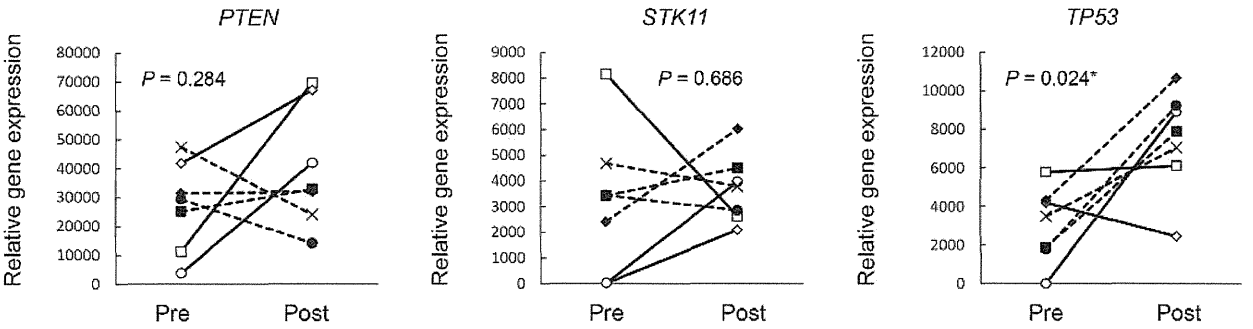

Figure 2: The results of the gene expression analysis of paired non-responder tumor samples. The gene expression levels were evaluated by RNA sequencing, and the expression was compared in paired pre- and post-chemoradiotherapy samples from nine non-responders. The expression of three major tumors suppressor genes (*PTEN*, *STK11* and *TP53*) in paired samples is shown. Paired t-tests were used for the statistical analysis.

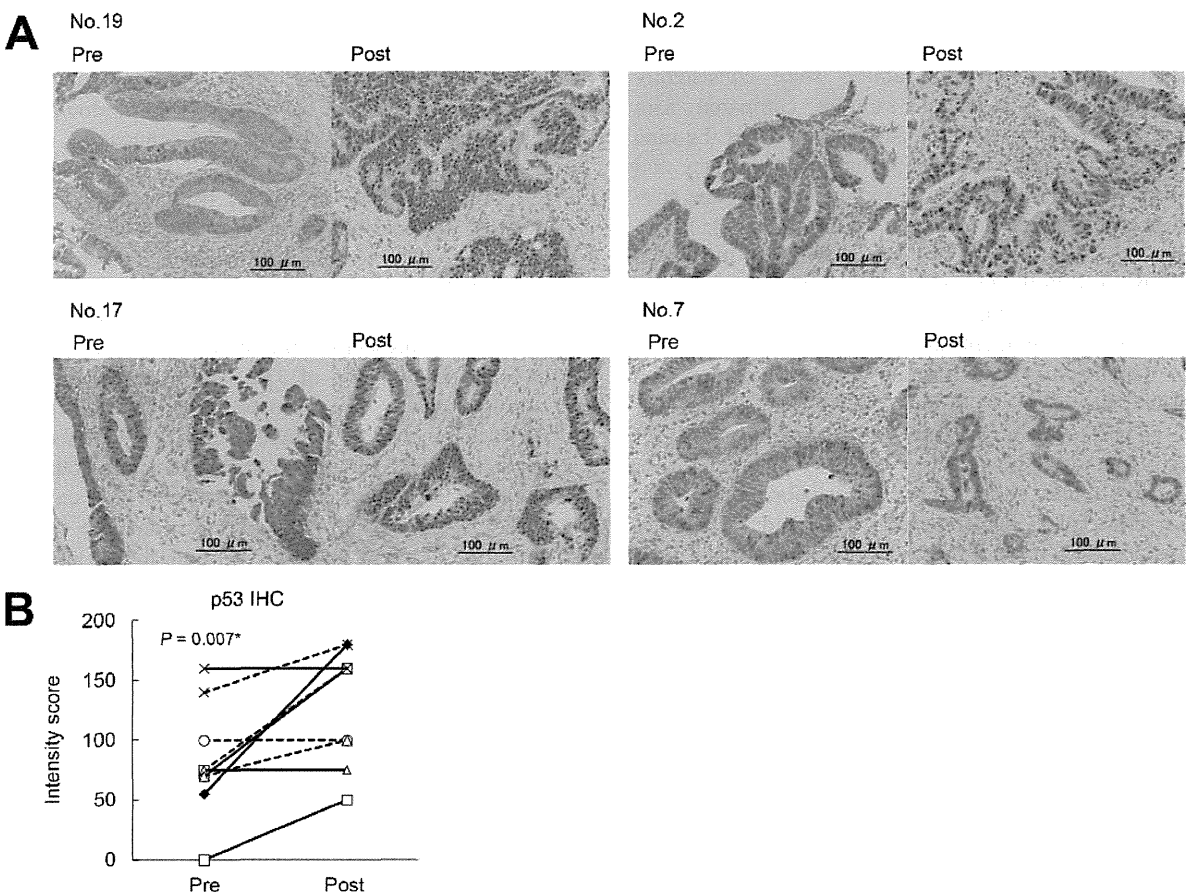

Figure 3: Immunohistochemical staining of paired tumor samples using an anti-p53 antibody. (**A**). Representative staining for p53 in paired non-responder samples. (original magnification, x25). No.19 and No.2 cases were increased p53 staining group. No.17 and No.7 cases were no change group. (**B**). The scores for p53 staining were compared between pre- and post-chemoradiotherapy samples. The intensity score = (average of area (%) x intensity of staining (0-2). Paired t-tests were used for the statistical analysis.